
SurgTEMP: Temporal-Aware Surgical Video Question Answering with Text-guided Visual Memory for Laparoscopic Cholecystectomy

 Shi Li ^{a,*}, Vinkle Srivastav ^a, Nicolas Chanel ^a, Saurav Sharma ^a, Nabani Banik ^a, Lorenzo Arboit ^a, Kun Yuan ^a, Pietro Mascagni ^{a,c,1}, Nicolas Padoy ^{a,1}

^aUniversity of Strasbourg, CNRS, INSERM, ICube, UMR7357, Strasbourg, France

^bIHU Strasbourg, Strasbourg, France

^cFondazione Policlinico Universitario Agostino Gemelli IRCCS, Rome, Italy

ABSTRACT

Surgical procedures are inherently complex and risky, requiring extensive expertise and constant focus to well navigate evolving intraoperative scenes. Computer-assisted systems such as surgical visual question answering (VQA) offer promises for education and intraoperative support. Current surgical VQA research largely focuses on static frame analysis, overlooking rich temporal semantics. Surgical video question answering is further challenged by low visual contrast, its highly knowledge-driven nature, diverse analytical needs spanning scattered temporal windows, and the hierarchy from basic perception to high-level intraoperative assessment. To address these challenges, we propose *SurgTEMP*, a multimodal LLM framework featuring (i) a query-guided token selection module that builds hierarchical visual memory (spatial and temporal memory banks) and (ii) a Surgical Competency Progression (SCP) training scheme. Together, these components enable effective modeling of variable-length surgical videos while preserving procedure-relevant cues and temporal coherence, and better support diverse downstream assessment tasks. To support model development, we introduce CholeVidQA-32K, a surgical video question answering dataset comprising 32K open-ended QA pairs and 3,855 video segments (approximately 128 h total) from laparoscopic cholecystectomy. The dataset is organized into a three-level hierarchy—Perception, Assessment, and Reasoning—spanning 11 tasks from instrument/action/anatomy perception to Critical View of Safety (CVS), intraoperative difficulty, skill proficiency, and adverse event assessment. In comprehensive evaluations against state-of-the-art open-source multimodal and video LLMs (fine-tuned and zero-shot), SurgTEMP achieves substantial performance improvements, advancing the state of video-based surgical VQA.

KEYWORDS: Surgical Video Question Answering, Surgical Safety Assessment, Multimodal Large Language Model.

*Corresponding author

¹These authors contributed equally as co-last authors.

1. Introduction

Surgery is a highly complex and skill-demanding discipline, characterized by substantial risk and a prolonged training period before practitioners achieve proficiency. At the beginning of training, a solid understanding of anatomy is generally assumed, as it provides the foundation for interpreting the operative field, for example the identification of key anatomical landmarks and the assessment of their status. Based on that, years of residency are typically required to master fundamental operative actions, such as suturing and tissue retraction, and to develop the ability to perform context-aware intraoperative assessments. For instance, in laparoscopic cholecystectomy surgeons must judge whether the cystic duct has been adequately dissected and exposed and whether it is safe to divide it. This competence is typically acquired only after numerous procedures. Such skill is essential for ensuring a smooth operation, minimizing complications, and achieving favorable postoperative outcomes.

Recent advances in surgical data science have endeavored to capture the aforementioned nuances in surgery. A substantial body of work has explored the perception of the surgical scene, including tools (Allan et al., 2019; Nwoye et al., 2019; da Costa Rocha et al., 2019; Hasan et al., 2021; Wagner et al., 2023; Tao et al., 2023; Zia et al., 2025), anatomy (Vlontzos et al., 2019; Ali et al., 2021; Meyer et al., 2025; Murali et al., 2025), and surgical actions (Nwoye et al., 2020, 2022; Sharma et al., 2023a; Hu et al., 2024; Pei et al., 2025; Ayobi et al., 2025). Beyond these foundational efforts in surgical scene understanding, work has also emerged focusing on more complex assessments of additional facets of surgery. One notable line of work centers on the Critical View of Safety (CVS) (Mascagni et al., 2020), a standardized checklist for specific procedures such as laparoscopic cholecystectomy. By ensuring that key anatomical landmarks are clearly dissected and exposed, CVS adherence reduces the risk of inadvertent injury to critical structures. Vision-based models have been proposed to predict CVS achievement by leveraging intraoperative visual cues (Murali et al., 2023b,a; Alapatt et al., 2024; Jaspers et al., 2025), offering automated support for this essential safety protocol. Another promising direction involves LCOD (Laparoscopic Cholecystectomy Operative Difficulty) assessment (Vannucci et al., 2022; Sharma et al., 2025). Scoring systems have been introduced to quantify surgical difficulty based on observable intraoperative findings (e.g., visceral fat, where thick adipose tissue may obscure anatomical landmarks and hinder instrument manipulation), providing decision support for critical choices such as whether to involve more experienced practitioners or to convert from a laparoscopic to an open approach. Additionally, intraoperative adverse event (IAE) detection models (Bose et al., 2025) have been developed to identify unexpected or undesirable incidents during surgery, including bleeding, mechanical injuries, and other deviations from the ideal intraoperative course. Moreover, surgical skill assessment (Wagner et al., 2021; Pedrett et al., 2023) is a well developed modeling task that facilitates the quantification of proficiency levels in tissue manipulation, suturing, and other technical skills.

The intraoperative assessments highlighted above are inherently dynamic: they unfold progressively and can only be fully interpreted within a temporal context. Apart from the aforementioned vision-only solutions, surgical VQA systems have

emerged as promising intraoperative analytical tools to support education by formulating detection tasks into interactive question-answering and reasoning processes between the user and the model, thereby offering greater flexibility and potential for broader applicability. Existing works—such as Surgical-VQA (Seenivasan et al., 2022), Surgical-VQLA (Bai et al., 2023b), SSG-VQA (Yuan et al., 2024), and PitVQA (He et al., 2024)—have laid the foundation for this line of research by exploring the capability of VQA systems to reason about the detection and grounding of key elements (e.g., tools, anatomy, actions) in static frames from surgical videos. However, despite this promising potential, the dynamic information embedded in temporal context remains underexplored, even though it is essential for various intraoperative analytical needs, thereby limiting the practical applicability of such systems.

Addressing this gap and developing surgical video question answering systems for diverse practical intraoperative analytic needs presents several significant challenges.

First—domain-specific visual interpretation: Unlike natural images or videos, where visual semantics (i.e., objects and their defining attributes such as edges and color) are often clear and dominant, endoscopic surgical videos pose a unique challenge. Here, anatomical structures often lack strong visual contrast, and the identification of anatomical boundaries, tissue types, or pathological states often relies on domain-specific priors. Surgeons, for instance, infer granular anatomical elements by triangulating contextual information—such as procedure type, surgical phase, and the relative positions of known landmarks—alongside subtle visual cues and their understanding of typical spatial relationships and expected tissue behavior.

Second—variable spatiotemporal granularity needs: Throughout the operation, numerous assessments are performed across many timespans with significantly different granularity needs. For example, the detection of LCOD findings and IAE usually requires the identification of shorter-duration events with finer granularity because they are often related to the status of anatomical landmarks, which rely on subtle visual cues such as shape and texture. In contrast, skill assessment needs a longer observation window to draw conclusions about proficiency based on the smoothness of operation and near-misses. This requires the model to have stronger spatiotemporal understanding capabilities that adapt to these various needs.

Third—hierarchical task dependencies: All types of intraoperative assessments rely on the fundamental capabilities of interpreting the operative field, which form a clear hierarchical structure in which sequential atomic surgical scene understandings support higher-level assessments. For example, CVS relies on the clear identification of fully dissected and exposed anatomical landmarks.

To address these challenges, we propose a novel surgical video QA framework named *SurgTEMP*. It is a multimodal LLM-based framework that contains a visual feature extraction module and textual tokenization to produce tokens from both modalities and feed them into a backbone LLM to generate textual responses as shown in Figure 1. At its core is a **TEMP (TE**xt-guided **M**emory **P**yrAmid) constructor—a cross-modal learnable visual token arrangement module specifically designed to balance two key aspects in the knowledge-intensive surgical domain. First, it captures fine-grained details in short yet significant spatiotemporal contexts via a spatial memory

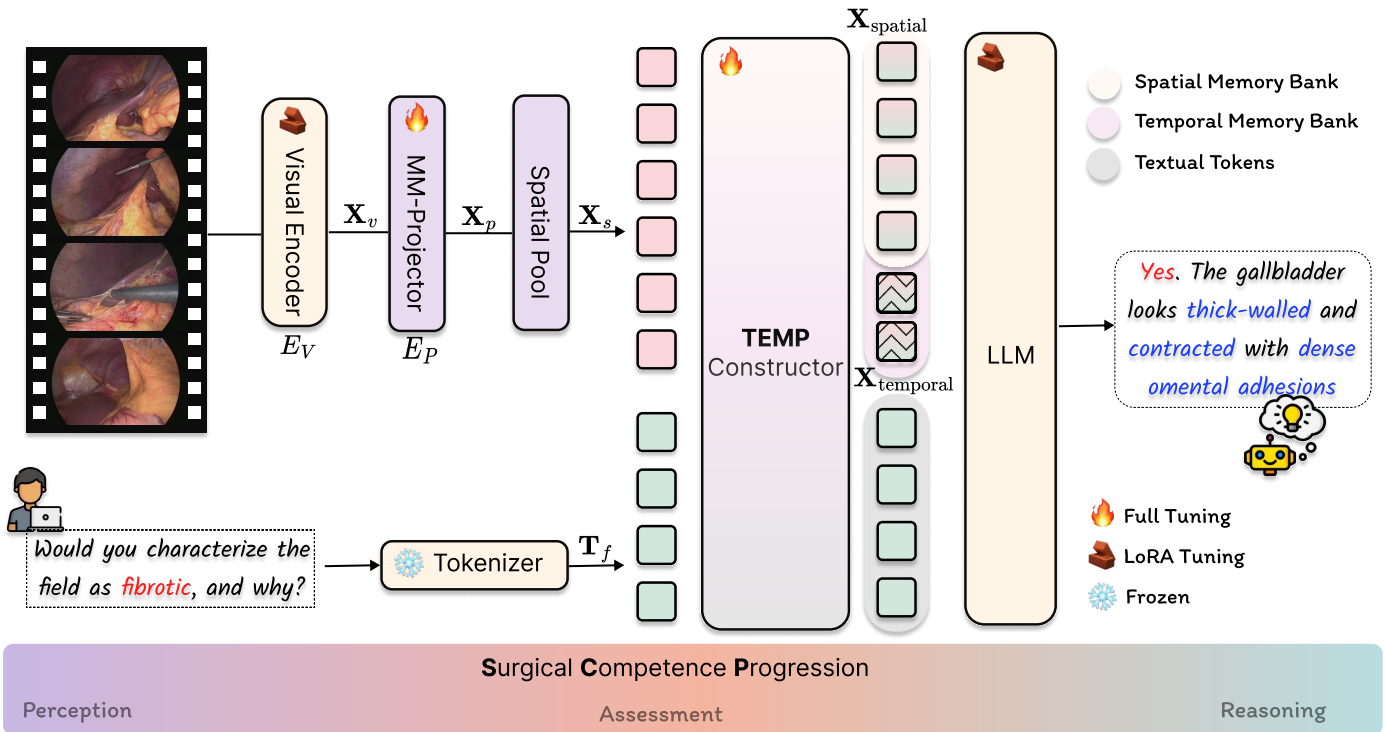


Fig. 1: Architecture Overview of Our Proposed Model SurgTEMP. The sampled video frames first go through a feature extraction pipeline containing visual encoder, multi-modal projector and spatial pooling to obtain visual tokens X_s . Textual input is processed through the textual tokenizer to yield textual tokens T_f . Our proposed TEMP constructor takes tokens from both modalities to construct a hierarchical visual memory bank including spatial and temporal granularity. Then an LLM is employed as backbone to generate answers conditioned on visual input and textual query.

bank (e.g., proper dissection to expose critical anatomy). Second, it preserves lengthy spans of progressive analytical signals via a temporal memory bank (e.g., skill proficiency assessment over a surgical phase, reflecting cumulative decision points in operative field manipulation). Additionally, a domain-specific training scheme—Surgical Competence Progression (SCP)—progressively builds the model’s capabilities from fundamental perception to higher-level assessment and reasoning tasks.

The design choices and training strategy directly address the aforementioned domain challenges. *First*, by utilizing the textual query as the guiding signal, the model learns to form informative spatial memory banks that benefit from the embedded knowledge in the pretrained backbone MLLM and accommodate the domain shift in the downstream fine-tuning dataset, which mitigates the challenge of limited visual contrast and takes advantage of the knowledge-driven nature of surgical videos. *Second*, by constructing a hierarchical memory bank that covers fine-grained and short-term memory as well as long-term yet coarser memory, our model gains enhanced capabilities for handling variable spatiotemporal attentional needs from different assessment tasks. *Third*, the SCP training scheme progressively trains the model from fundamental perception tasks to higher-level assessment and reasoning tasks, directly addressing the challenge of hierarchical task dependencies by explicitly modeling the structure in which basic surgical scene understanding serves as a prerequisite for more complex intraoperative assessments.

Moreover, to facilitate model training and evaluation, we introduce CholeVidQA-32K, an instruction-tuning dataset that distinguishes itself from existing resources through dynamic temporal context and broader assessment coverage (Table 1).

To address the challenge in the surgical domain regarding the hierarchical nature of intraoperative assessments, we formulate and organize 11 tasks into a three-level hierarchy (Figure 2).

At the *Perception* level, we design three fundamental tasks for surgical scene understanding. *Tool Perception* facilitates contextually dynamic responses that reference tools by position and movement. *Action Perception* captures surgical actions with clinical rationale. *Anatomical Structure Perception* provides fine-grained descriptions of anatomical landmarks, including attributes such as status, position, shape, and color. Data for this level is derived from the CholecT50 (Nwoye *et al.*, 2022) dataset, where we segment videos by action continuity and incorporate structured caption annotations from clinicians, repurposed into semantically rich QA pairs. These short-span video segments preserve action-oriented visual dynamics. Together, these three tasks establish fundamental visual recognition capabilities for surgical scenes.

At the *Assessment* level, we design tasks to support diverse intraoperative analysis needs, including *Critical View of Safety*, *Difficulty Findings*, *Skills Proficiency* and *Adverse Events* assessments. These tasks encompass different analytical scenarios and predictive formulations, including binary and multi-category classification. Data for this level is sourced from Endoscapes (Mascagni *et al.*, 2025) and CholeScore (Sharma *et al.*, 2025). We segment Endoscapes videos using fixed 5-second intervals and CholeScore videos by surgical phase, resulting in two distinct temporal scales—shorter clips for fine-grained assessment and longer segments spanning minutes to tens of minutes for comprehensive evaluation. We transform existing categorical annotations into open-ended question-answer pairs with enriched descriptive explanations.

Finally, at the *Reasoning* level, we support more complex

clinical analysis by combining operative field interpretation and assessments across video segments. With the assistance of large language models (LLMs), we generate condensed descriptive QA pairs on basic scene understanding (i.e., *Surgical Scene Description*) and on various intra-operative assessment analysis (i.e., *Comprehensive Assessment*). To further stimulate the models' reasoning capability, we create reasoning questions by conditioning on action intentions (i.e., *Action Rationale Reasoning*) and intraoperative variables (i.e., *Intra-operative Planning*), enabling scenario-based analysis.

We evaluate our proposed model using three tiers of metrics: classification metrics reflecting categorical capability, overlap metrics reflecting textual alignment with ground-truth answers, and multifaceted LLM-based scores reflecting response quality across multiple dimensions including correctness, relevance, and linguistic quality.

Experimental results broken down across multiple levels show that our model outperforms strong general-domain video QA baselines under both fine-tuned and zero-shot settings on our dataset, with notable margins on longer and more complex tasks.

Furthermore, to validate the real-world applicability of our model, we develop a golden set consisting of a carefully selected subset of videos and questions from the test set, annotated with high-quality answers manually written by clinicians that reflect more visually and clinically grounded reasoning processes. Experimental results on the golden set reveal that our model achieves better alignment with clinician-curated answers compared to all baselines, demonstrating its potential for supporting clinical education and decision-making in real surgical settings.

Our contributions can be summarized as follows:

- We propose SurgTEMP, a model capable of handling variable-length surgical videos and tasks requiring different granularities of visual cues, advancing the state of surgical video question answering.
- We introduce a novel surgical video question answering dataset, CholeVidQA-32K, featuring dynamic temporal context and broad task coverage, facilitating video-based visual question answering research across various downstream applications.
- We evaluate our model on a carefully curated golden test set with high-quality answers manually written by clinicians, reflecting real-world intraoperative assessment reasoning. Results show superior alignment of our model compared to all baselines.

2. Related work

2.1. Surgical Computer Vision for Laparoscopic Videos

Recent advances in deep learning have enabled sophisticated modeling of intraoperative dynamics, particularly in laparoscopic surgery, establishing the foundation for contemporary surgical computer vision research. The field has evolved to address surgical scene understanding across multiple levels of semantic granularity. Significant attention has been directed toward action triplet recognition (Nwoye et al., 2020, 2022, 2023; Sharma et al., 2023a,b; Hu et al., 2024; Pei et al., 2025;

Ayobi et al., 2025), which involves predicting structured tool-action-anatomy relationships (e.g., grasper-grasp-gallbladder) from video sequences and is commonly formulated as a structured multi-label set prediction problem at the frame or short-clip level. A representative benchmark is CholecT50 (Nwoye et al., 2022), which provides frame-level tool-action-anatomy triplet annotations for laparoscopic cholecystectomy videos. Complementing these temporal modeling efforts, the detection and tracking of anatomical structures (Vlontzos et al., 2019; Ali et al., 2021; Luengo et al., 2022; Meyer et al., 2024, 2025) and surgical instruments (Allan et al., 2019; Nwoye et al., 2019; da Costa Rocha et al., 2019; Hasan et al., 2021; Wagner et al., 2023; Tao et al., 2023; Zia et al., 2025) have been extensively studied, typically formulated as object detection and semantic segmentation tasks.

Recognizing the high-stakes nature of laparoscopic surgery, researchers have increasingly focused on data-driven approaches to capture and enhance surgical safety. A prominent line of research centers on the Critical View of Safety (CVS), a procedure-specific checklist designed to guide surgeons in achieving clear visual exposure of critical anatomical landmarks, thereby minimizing the risk of inadvertent injuries such as bile duct damage during laparoscopic cholecystectomy (Mascagni et al., 2021b). The annotation process for CVS assessment typically requires expertise from multiple levels of clinical experience and adherence to detailed protocols (Mascagni et al., 2021a) to ensure consistency and minimize inter-annotator variability. The Endoscapes dataset (Mascagni et al., 2025) was developed to support this research direction, providing 201 laparoscopic videos with binary CVS labels at fixed 5-second intervals indicating whether each of the three established criteria is achieved, along with sparse bounding box and segmentation mask annotations. Models including LG-CVS (Murali et al., 2023b) and Jumpstart (Alapatt et al., 2024) have been developed using this dataset to predict the achievement of each criterion, facilitating automated CVS assessment.

Apart from CVS evaluation, surgical difficulty assessment has emerged as another critical safety consideration. Established scoring systems, such as the Nassar and Sugrue scores and the Parkland Grading Scale (PGS), quantify procedural complexity based on intraoperative findings. Recent computational approaches, including SurgPrOD (Sharma et al., 2025), have demonstrated the feasibility of predicting difficulty levels from early-stage surgical videos and introduced CholeScore, which provides videos annotated with the binary presence of difficulty findings across three scales. Additionally, the detection of intraoperative adverse events (IAE)—such as bleeding and mechanical injuries—represents a crucial component of surgical safety monitoring. These events, while potentially emergent, have significant implications for surgical outcomes. Recent work, including BetaMixer (Bose et al., 2025), has explored automated detection of such events in gastric bypass procedures. Moreover, automated surgical skill assessment has emerged as a promising research direction for understanding and improving the human factor in the operating room (Gao et al., 2014; Liu et al., 2021). Most works use the OSATS (Martin et al., 1997) protocol to evaluate proficiency levels for surgical operations.

Our dataset curation pipeline leverages existing videos from prior vision-centric datasets, including CholecT50, En-

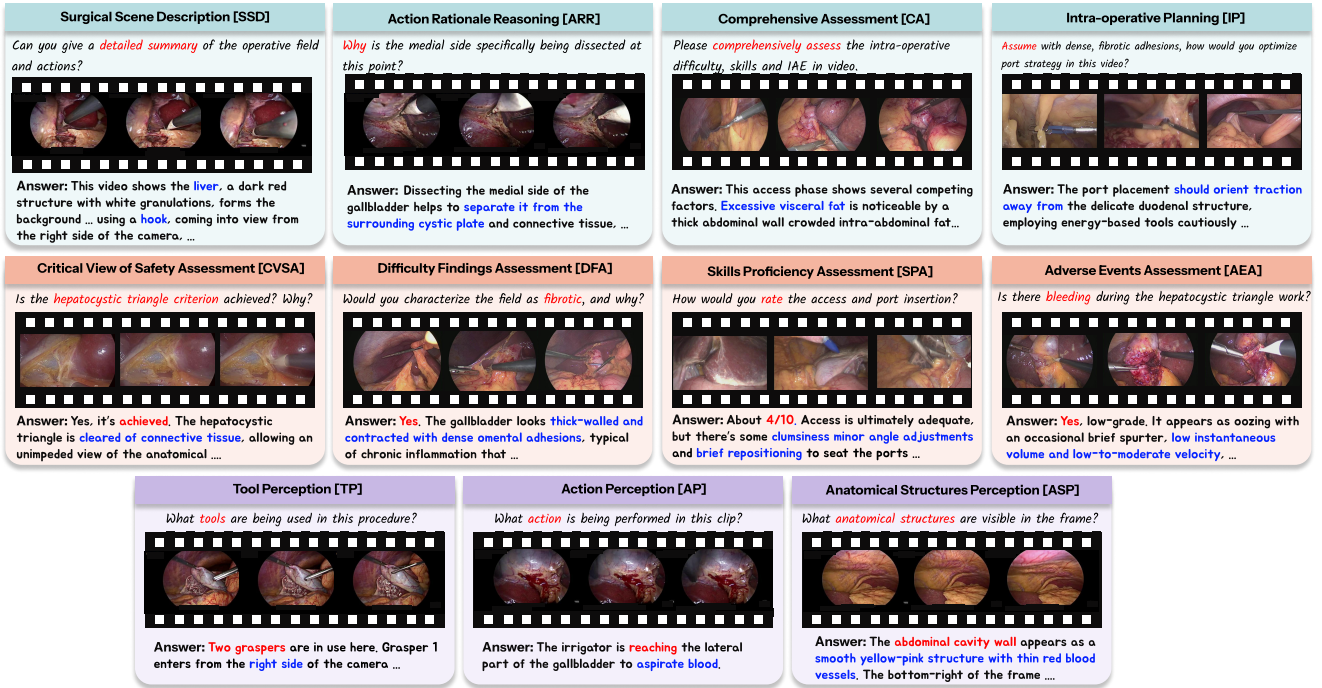


Fig. 2: Hierarchical overview of the CholeVidQA-32K dataset. The 11 tasks are categorized into three capability levels: **Perception** (basic surgical scene understanding), **Assessment** (surgical assessment for multiple ends), and **Reasoning** (complex surgical scene analysis). In the question and answer examples, text indicating task-specific characteristics is shown in red, while descriptive elements are highlighted in blue.

doscapes, and CholeScore. For generic surgical scene perception, we adopt clinician-annotated captions to provide visually contextual textual descriptions. For higher-level intra-operative assessments, in light of the high annotation cost, we repurpose existing structured labels into open-ended question-answer pairs and incorporate enriched descriptions from annotation definitions. Although our QA pairs are derived from these existing labels, the proposed tasks differ fundamentally from the original visual-centric formulations: they require generating open-ended, and explanatory, natural language answers conditioned on questions. Consequently, we focus on comparisons within the VQA formulation (including strong multimodal LLM baselines) and regard prior visual-centric works as complementary foundations for label curation rather than directly competing baselines.

2.2. Multimodal Large Language Models

The emergence of Large Language Models (LLMs) has significantly transformed artificial intelligence capabilities (OpenAI *et al.*, 2024; DeepSeek-AI *et al.*, 2025), which have demonstrated remarkable world knowledge and reasoning capabilities acquired through training on vast textual corpora, fundamentally enhancing human-AI interaction and problem-solving potential. The critical aspects of these models are the multimodal understanding. A common design is the encoder alignment approach (Liu *et al.*, 2023; Ye *et al.*, 2024; Zhu *et al.*, 2023; Li *et al.*, 2023b, 2025; Laurençon *et al.*, 2024; Lin *et al.*, 2024b), which leverage strong pretrained vision encoders with lightweight adapters to align image features to an LLM. Another family uses a unified pretraining paradigm, where both image and text modalities are jointly trained from the start to ensure deeper integration (Bai *et al.*, 2023a; Li *et al.*, 2022; Alayrac *et al.*, 2022; Chen *et al.*, 2023b,a; Huang *et al.*, 2023; Peng *et al.*, 2023).

Extending beyond static image understanding, one line of work on video-enabled multimodal LLMs (Maaz *et al.*, 2024b; Li *et al.*, 2024a) builds upon image-focused frameworks and treats a sequence of frames as a set of independent images. A second line explicitly introduces a dedicated encoder for video input (Li *et al.*, 2024b; Lin *et al.*, 2024a). To address the challenges posed by long-form video and the limited context window of LLMs, recent models adopt diverse architectural strategies. mPLUG-Owl3 (Ye *et al.*, 2024) introduces a hyper-attention block as a fundamental architectural change for improved cross-modal fusion. LLaVA-Video (Zhang *et al.*, 2025) incorporates a slow-fast visual feature pooling scheme with multiple strides to provide two levels of visual granularity. InternVideo2.5 uses token-merging and dropout to reduce the number of visual tokens and extend the effectively perceivable video length. LongVA transfers reasoning capabilities from image pretraining and scales the model at test time for long-context analysis by representing video as multi-grid images.

Our method is a domain-tailored extension of recent video LLM architectures. It departs from prior work through a text-guided hierarchical memory bank that jointly maintains fine- and coarse-grained surgical visual representations, balancing localized operative field interpretations with broader procedural context. This design foregrounds knowledge-driven cues (e.g., anatomical landmarks) that are less visually salient yet conceptually defined, in contrast to general-domain settings. Accordingly, we benchmark against open-source video LLMs to demonstrate the effectiveness of our architecture in capturing surgical nuance.

2.3. Visual Question Answering: From General Domain to Surgery

Visual Question Answering (VQA) has played a pivotal role in advancing multimodal understanding, with large-scale

Table 1: Comparison of surgical VQA datasets. Our dataset distinguishes itself through video-based input, significantly longer average word count, and comprehensive coverage across perception, assessment, and reasoning tasks.

Dataset	Visual Input	Average Word Count	Perception tasks	Assessment tasks	Reasoning tasks
EndoVis-18-VQA (Seenivasan et al., 2022)	image	5.8	✓	✗	✗
Cholec80-VQA (Seenivasan et al., 2022)	image	2.0	✓	✗	✗
SSG-VQA (Yuan et al., 2024)	image	12.8	✓	✗	✗
PitVQA (He et al., 2024)	image	10.3	✓	✗	✗
Surg-396K (Wang et al., 2025a)	image	-	✓	✗	✓
CholeVidQA-32K	video	70.5	✓	✓	✓

datasets providing the foundation for training and evaluation across diverse scenarios. The VQA v1 and v2 datasets (Agrawal et al., 2016) were among the earliest benchmarks, pairing open-ended questions with natural images to establish the fundamental paradigm. Subsequent developments introduced increasingly sophisticated challenges: GQA (Hudson and Manning, 2019) emphasized compositional reasoning and scene graph grounding, while VizWiz (Gurari et al., 2018) introduced real-world complexity through images captured by visually impaired users. The field further evolved toward knowledge-intensive reasoning with datasets like OK-VQA (Marino et al., 2019) and A-OKVQA (Schwenk et al., 2022), which required external knowledge integration and commonsense understanding. More recently, with the emergence of multimodal large language models, comprehensive evaluation suites such as MM-Bench (Liu et al., 2024), SEED-Bench (Li et al., 2023a), and MM-Vet (Yu et al., 2024) have been developed to systematically assess capabilities spanning perception, reasoning, and instruction-following across diverse scenarios.

Building upon these general-domain foundations, surgical visual question answering has emerged as a specialized paradigm that adapts VQA principles to address the unique challenges of surgical environments, offering promising potential for developing flexible interfaces and educational tools that bridge computer vision and natural language understanding in clinical contexts. Surgical-VQA (Seenivasan et al., 2022) pioneered this research direction by leveraging existing annotations from the EndoVis17 and EndoVis18 datasets (Allan et al., 2019) to create question-answer pairs focused on instrument recognition and basic scene understanding. Building upon this foundation, Surgical-VQLA (Bai et al., 2023b) extended the framework by incorporating visual grounding capabilities, enabling models to localize relevant regions while answering questions. SSG-VQA (Yuan et al., 2024) further enhanced spatial reasoning by integrating scene graphs as additional input modalities to improve the model’s spatial awareness and relational understanding. The scope of surgical VQA has also expanded beyond cholecystectomy procedures, with PitVQA (He et al., 2024) extending the paradigm to pituitary surgery, demonstrating the generalizability of the approach across different surgical procedures. More recently, EndoChat (Wang et al., 2025a) has attempted to unify various spatial recognition tasks within a comprehensive VQA framework.

Despite these advances, existing surgical VQA systems remain predominantly focused on single-frame analysis and generic scene-understanding tasks. Our work extends this paradigm by introducing video-based input and broader coverage of assessment tasks, including safety- and procedure-oriented reasoning. Because prior models are predominantly

trained on static imagery and are not optimized for temporal integration, their reported performance does not necessarily reflect capabilities under video-based evaluation. Accordingly, we position earlier systems as conceptual precedents rather than directly comparable modeling baselines.

3. Methodology

3.1. SurgTEMP

3.1.1. Modeling Pipeline Overview

As shown in Figure 1, the architecture comprises four key components working synergistically: (1) a *SigLIP Visual Encoder* (Zhai et al., 2023) employing a Vision Transformer for patch-based feature extraction; (2) a *Multi-Modal Projector* with spatial pooling that bridges visual and textual representation spaces; (3) a novel *Text-Guided Memory Pyramid (TEMP)* module that constructs hierarchical visual memories through cross-modal attention and differentiable frame selection; and (4) a *Qwen2-7B Large Language Model* backend for multimodal fusion and response generation.

Our key contribution lies in the TEMP constructor module, which dynamically selects the most relevant frames using Gumbel-Softmax mechanisms and constructs a dual-granularity memory pyramid comprising both fine-grained spatial details for operative field analysis and coarse-grained temporal context for procedural awareness. This hierarchical representation is enhanced by learnable separator tokens that adaptively encode spatial-temporal boundaries between patch tokens. We employ a hybrid parameter optimization strategy combining parameter-efficient LoRA adapters for heavily parameterized components (visual encoder and LLM backbone) with full fine-tuning for lightweight architectural elements (multi-modal projector and separator tokens), enabling effective domain adaptation while maintaining computational efficiency.

3.1.2. Visual Feature Extraction

Uniform Frame Sampling Strategy: To effectively process surgical videos of varying durations while maintaining computational efficiency, we employ a uniform frame sampling strategy that preserves temporal consistency across different video lengths. For each input video, we sample a fixed number of frames T at regular intervals throughout the entire temporal sequence. The uniform sampling interval $\Delta\tau = \frac{L}{T-1}$ is computed based on the video length L and desired frame count T , allowing the model to capture both fine-grained procedural details in short segments and long-range temporal dependencies in extended surgical phases. This strategy ensures that critical safety-relevant visual cues are systematically preserved across

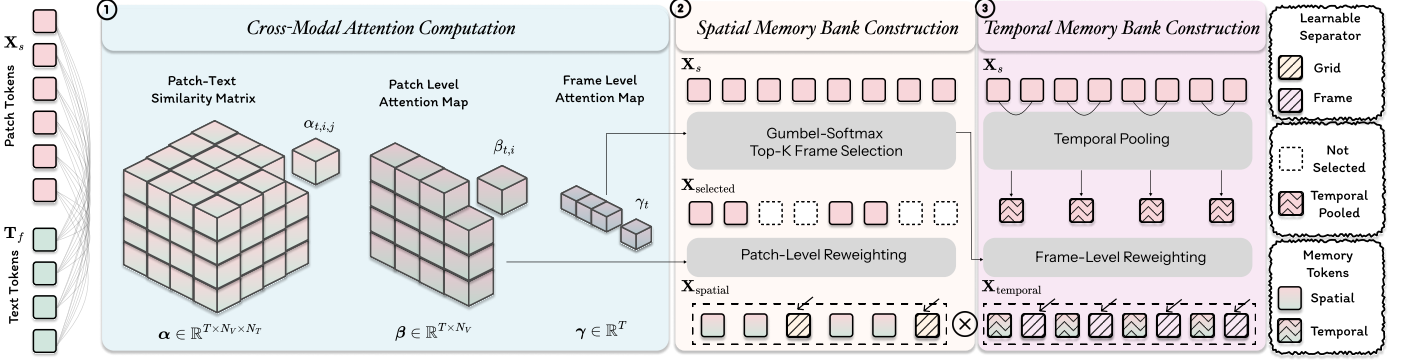


Fig. 3: Illustration of our proposed TEMP module. It contains three processing steps. First, multi-level text-visual attention maps are computed. Second, the spatial memory bank is constructed by selecting frames based on frame-level attention and reweighting visual tokens with the patch-level attention map. Third, the temporal memory bank is formed by temporal pooling and reweighting with the frame-level attention map.

the temporal dimension while maintaining manageable computational complexity.

SigLIP Visual Encoder: The visual encoding process begins with input video frames $\mathbf{X} \in \mathbb{R}^{T \times C \times W \times H}$, where T , C , W , and H respectively denote the number of uniformly sampled frames, color channels, frame width, and frame height. The visual encoder processes each frame independently through patch-based tokenization, dividing individual frames into non-overlapping spatial patches:

$$E_V : \mathbb{R}^{T \times C \times W \times H} \rightarrow \mathbb{R}^{T \times M \times D_V} \quad (1)$$

in which the input frames are transformed into dense visual representations:

$$\mathbf{X}_V = E_V(\mathbf{X}) \quad (2)$$

where M represents the total number of spatial patches per frame and D_V denotes the dimensionality of the visual embedding space.

Multi-Modal Projector: The multi-modal projector serves as a critical alignment component that bridges the domain gap between vision-specific and language-specific representation spaces, which is formally defined as:

$$E_p : \mathbb{R}^{T \times M \times D_V} \rightarrow \mathbb{R}^{T \times M \times D} \quad (3)$$

where D represents the target embedding dimension shared between visual and textual modalities. The projector is implemented as a multi-layer perceptron (MLP) with non-linear activations between layers:

$$\begin{aligned} h^{(0)} &= \mathbf{X}_V \\ h^{(i)} &= \text{GELU}(W_i h^{(i-1)} + b_i), \quad i = 1, \dots, L-1 \\ \mathbf{X}_p &= W_L h^{(L-1)} + b_L \end{aligned} \quad (4)$$

where $h^{(i)}$ denotes the hidden representation at the i -th layer, L represents the total number of layers, W_i and b_i are the learnable weight matrix and bias term for the i -th layer, and GELU denotes the Gaussian Error Linear Unit activation function. The final projected visual representation $\mathbf{X}_p \in \mathbb{R}^{T \times M \times D}$ is obtained after L layers of transformation.

Spatial Pooling: To balance computational efficiency with spatial detail preservation, we subsequently apply spatial pooling operation that reduces the spatial resolution while maintaining essential visual information. The spatial pooling transformation is formally defined as:

$$\text{Spatial_Pool} : \mathbb{R}^{T \times M \times D} \rightarrow \mathbb{R}^{T \times N_V \times D} \quad (5)$$

with stride parameter p , yielding spatially-reduced visual representations:

$$\mathbf{X}_s = \text{Spatial_Pool}(\mathbf{X}_p) \quad (6)$$

where $N_V = \frac{M}{p^2}$ represents the reduced number of visual tokens per frame, effectively managing the trade-off between spatial granularity and computational complexity. These spatially-reduced representations \mathbf{X}_s serve as input to the subsequent TEMP constructor.

3.1.3. Text Processing Pipeline

For textual input processing, we follow the implementation in Qwen2's tokenizer. The text processing differs between training and inference to accommodate distinct input configurations. During training, the textual input consists of both question \mathbf{Q}_{ues} and ground-truth answer \mathbf{A}_{ns} sequences concatenated as $\mathbf{S}_{\text{train}} = [\mathbf{Q}_{\text{ues}}, \langle \text{sep} \rangle, \mathbf{A}_{\text{ns}}]$ to enable supervised learning through teacher forcing. During inference, only the question sequence \mathbf{Q}_{ues} is provided as input for autoregressive response generation. The processing begins with tokenization using the pre-trained tokenizer \mathcal{T} , which segments the input sequence into discrete tokens: $\{\tau_1, \tau_2, \dots, \tau_{N_T}\} = \mathcal{T}(\mathbf{S})$, where N_T represents the total number of textual tokens and \mathbf{S} denotes either $\mathbf{S}_{\text{train}}$ or \mathbf{Q}_{ues} depending on the stage.

The tokens are then transformed into dense embeddings via the embedding layer: $\mathbf{T} = E_T(\{\tau_1, \dots, \tau_{N_T}\}) \in \mathbb{R}^{N_T \times D}$, where $E_T : \mathbb{R}^{N_T} \rightarrow \mathbb{R}^{N_T \times D}$ represents the token embedding transformation. To incorporate positional information, Rotary Position Embedding (RoPE) is employed to the embeddings using position-dependent rotation angles $\theta_i = 10000^{-2i/D}$ for each dimension pair. The final positional-encoded textual representations are obtained as $\mathbf{T}_f = \text{RoPE}(\mathbf{T}, \{1, 2, \dots, N_T\})$, where D denotes the unified embedding dimension shared between textual and visual modalities.

3.1.4. Text-Guided Memory Pyramid

With the textual tokens \mathbf{T}_f and visual tokens \mathbf{X}_s , TEMP constructor will go through three steps, namely cross modal attention computation, spatial memory bank construction, and temporal memory construction, to build the final visual memory pyramid \mathbf{X}_f . Critically, during this process, answer tokens are masked to prevent the model from using future answer information to guide visual attention, ensuring that only question tokens contribute to the construction of the visual memory pyramid.

Cross-Modal Attention Computation: The TEMP module employs a hierarchical attention mechanism that computes cross-modal similarity between textual representations $\mathbf{T}_f \in \mathbb{R}^{N_T \times D}$ and spatially-reduced visual representations $\mathbf{X}_s \in \mathbb{R}^{T \times N_V \times D}$, progressively aggregating from fine-grained patch-text interactions to frame-level importance scores.

Patch-Text Similarity Matrix: For each visual patch token $\mathbf{x}_{t,i} \in \mathbb{R}^D$ at frame t and spatial position i , we calculate the cosine similarity with respect to all textual tokens, yielding a comprehensive similarity tensor:

$$\alpha_{t,i,j} = \frac{\mathbf{x}_{t,i} \cdot \mathbf{t}_j}{\|\mathbf{x}_{t,i}\|_2 \cdot \|\mathbf{t}_j\|_2} \quad (7)$$

where $\alpha_{t,i,j} \in [-1, 1]$ represents the cosine similarity between the i -th visual patch in frame t and the j -th textual token embedding \mathbf{t}_j . This produces a fine-grained attention tensor $\alpha \in \mathbb{R}^{T \times N_V \times N_T}$ capturing all pairwise patch-text interactions.

Patch-Level Attention Map: The patch-level attention weight is obtained by aggregating similarities across all textual tokens:

$$\beta_{t,i} = \frac{1}{N_T} \sum_{j=1}^{N_T} \alpha_{t,i,j} \quad (8)$$

where $\beta_{t,i}$ represents the average cross-modal similarity between the i -th visual patch in frame t and all textual tokens, resulting in a patch-level attention map $\beta \in \mathbb{R}^{T \times N_V}$ that provides a measure of textual relevance for each spatial patch within the surgical scene.

Frame-Level Attention Map: To capture temporal dynamics while maintaining computational efficiency, we aggregate patch-level attention weights to derive frame-level importance scores. For each frame t , the frame-level attention weight is computed as:

$$\gamma_t = \frac{1}{N_V} \sum_{i=1}^{N_V} \beta_{t,i} \quad (9)$$

representing the average textual relevance of all spatial patches within that temporal frame, yielding a frame-level attention map $\gamma \in \mathbb{R}^T$ that encodes the temporal importance of each frame based on text-visual alignment.

Spatial Memory Bank Construction: Based on the patch and frame level attention map, visual tokens are further arranged to form the visual memory bank following steps below.

Differentiable Frame Selection: To enable learnable and efficient frame selection, we apply the Gumbel-Softmax mechanism to identify the top- k most relevant frames based on their frame-level attention scores:

$$\mathbf{s}_t = \frac{\exp((\gamma_t + g_t)/\tau)}{\sum_{t'=1}^T \exp((\gamma_{t'} + g_{t'})/\tau)} \quad (10)$$

where $\mathbf{s}_t \in [0, 1]$ represents the selection probability for frame t , $g_t = -\log(-\log(\mathcal{U}(0, 1)))$ denotes Gumbel noise sampled from the standard Gumbel distribution with $\mathcal{U}(0, 1)$ representing the uniform distribution over $[0, 1]$, and τ is the temperature parameter controlling the sharpness of the selection distribution. This produces a probability distribution $\mathbf{s} \in \mathbb{R}^T$ over all frames where $\sum_{t=1}^T \mathbf{s}_t = 1$, with each element indicating the likelihood of selecting the corresponding frame. This approach maintains differentiability during training while approximating discrete selection during inference, enabling end-to-end optimization of

the frame selection process. The selected frame indices are obtained by:

$$\{t_1, t_2, \dots, t_k\} = \text{TopK}(\mathbf{s}_1, \mathbf{s}_2, \dots, \mathbf{s}_T, k) \quad (11)$$

where $\text{TopK}(\cdot, k)$ returns the indices of the k frames with the highest selection probabilities, ensuring that only the most textually-relevant temporal segments are retained for subsequent processing.

Patch-Level Reweighting: After frame selection, we renormalize the patch-level attention weights among the selected patches using softmax:

$$\tilde{\beta}_{t,i} = \frac{\exp(\beta_{t,i})}{\sum_{(t',j) \in \mathbf{X}_{\text{selected}}} \exp(\beta_{t',j})} \quad (12)$$

where $\mathbf{X}_{\text{selected}} = \{(t, i) : t \in \{t_1, t_2, \dots, t_k\}, i \in \{1, 2, \dots, N_V\}\}$ denotes the set of all patch indices from the selected top- k frames, and $\tilde{\beta}_{t,i}$ represents the renormalized patch-level attention weight for the i -th patch in frame t . We then compute reweighted patch representations by applying the renormalized attention weights:

$$\hat{\mathbf{x}}_{t,i} = \tilde{\beta}_{t,i} \cdot \mathbf{x}_{t,i} \quad (13)$$

for all $(t, i) \in \mathbf{X}_{\text{selected}}$, where $\hat{\mathbf{x}}_{t,i}$ denotes the attention-reweighted visual patch token that emphasizes textually-relevant spatial regions.

Spatial Memory Bank: At the fine-grained level, we construct the spatial memory bank by concatenating the reweighted selected visual patch tokens from the top- k frames with learnable grid separator tokens $\mathbf{sep}_{\text{grid}} \in \mathbb{R}^D$. To preserve the spatial layout structure of the original frames, we organize patches into grid rows where $N_G = \sqrt{N_V}$ represents the number of patches per row, and insert grid separators after each complete row:

$$\begin{aligned} \mathbf{X}_{\text{spatial}} = & [\hat{\mathbf{x}}_{t_1,1}, \dots, \hat{\mathbf{x}}_{t_1,N_G}, \mathbf{sep}_{\text{grid}}, \\ & \hat{\mathbf{x}}_{t_1,N_G+1}, \dots, \hat{\mathbf{x}}_{t_1,2N_G}, \mathbf{sep}_{\text{grid}}, \\ & \dots, \\ & \hat{\mathbf{x}}_{t_1,(N_G-1)N_G+1}, \dots, \hat{\mathbf{x}}_{t_1,N_V}, \mathbf{sep}_{\text{grid}}, \\ & \hat{\mathbf{x}}_{t_2,1}, \dots, \hat{\mathbf{x}}_{t_k,N_V}] \end{aligned} \quad (14)$$

This spatial memory bank preserves fine-grained visual details essential for operative field perception, while the learnable grid separators adaptively encode spatial row boundaries within each frame, evolving during training to optimally represent the 2D spatial layout of surgical scenes.

Temporal Memory Bank Construction: To construct the temporal memory bank, we first perform temporal pooling to aggregate spatial information within each frame, then apply frame-level attention reweighting based on textual relevance.

Temporal Pooling: At the frame level, we compute temporally-aggregated representations through average pooling within each frame:

$$\mathbf{f}_t = \frac{1}{N_V} \sum_{i=1}^{N_V} \mathbf{x}_{t,i} \quad (15)$$

where $\mathbf{f}_t \in \mathbb{R}^D$ represents the aggregated feature representation for frame t , computed for all T frames in the video sequence.

Frame-Level Reweighting: To emphasize temporally relevant frames based on text-visual alignment, we first renormalize the frame-level attention weights among all frames using softmax:

$$\tilde{\gamma}_t = \frac{\exp(\gamma_t)}{\sum_{t'=1}^T \exp(\gamma_{t'})} \quad (16)$$

where $\tilde{\gamma}_t$ represents the renormalized frame-level attention weight for frame t among all T frames. We then compute reweighted frame representations:

$$\hat{\mathbf{f}}_t = \tilde{\gamma}_t \cdot \mathbf{f}_t \quad (17)$$

for all frames $t \in \{1, 2, \dots, T\}$.

Temporal Memory Bank: Finally, we construct the temporal memory bank by concatenating the reweighted frame representations with learnable temporal separator tokens $\mathbf{sep}_{\text{frame}} \in \mathbb{R}^D$. These learnable temporal separators adapt to capture procedure-specific temporal dynamics and enable the model to encode meaningful temporal transitions between surgical phases:

$$\mathbf{X}_{\text{temporal}} = [\hat{\mathbf{f}}_1, \mathbf{sep}_{\text{frame}}, \hat{\mathbf{f}}_2, \mathbf{sep}_{\text{frame}}, \dots, \hat{\mathbf{f}}_T] \quad (18)$$

where each $\hat{\mathbf{f}}_t$ corresponds to the reweighted aggregated representation of frame t . The temporal memory bank captures procedural flow and contextual dependencies.

Hierarchical Visual Memory Pyramid: The final hierarchical visual memory pyramid is constructed by concatenating both memory banks:

$$\mathbf{X}_f = [\mathbf{X}_{\text{spatial}}, \mathbf{X}_{\text{temporal}}] \in \mathbb{R}^{(k \cdot N_V + k \cdot N_G + 2T - 1) \times D} \quad (19)$$

where the dimensionality comprises $k \cdot N_V$ spatial memory tokens from the selected k frames, $k \cdot N_G$ learnable grid separator tokens for spatial structure encoding, T temporal memory tokens representing all frames, and $T - 1$ learnable frame separator tokens for temporal boundary delineation.

This dual-memory architecture enables simultaneous access to both microscopic anatomical details and macroscopic procedural context within a unified representation space. The learnable separator tokens further enhance this capability by adaptively encoding structural boundaries that align with surgical workflow patterns, making the memory pyramid particularly effective for intraoperative assessment tasks that demand both spatial precision and temporal reasoning capabilities.

3.1.5. Multimodal Fusion and Response Generation

The processed hierarchical visual memory pyramid \mathbf{X}_f is concatenated with textual representations \mathbf{T}_f to form the unified multimodal input sequence $\mathbf{Z} = [\mathbf{X}_f, \mathbf{T}_f] \in \mathbb{R}^{N_{\text{total}} \times D}$, where N_{total} represents the total sequence length combining visual and textual tokens.

Large Language Model Backend: We employ Qwen2-7B as our foundation large language model, denoted as $F_{\text{LLM}} : \mathbb{R}^{N_{\text{total}} \times D} \rightarrow \mathbb{R}^{N_{\text{total}} \times V}$, where V represents the vocabulary size. The LLM processes the multimodal sequence through its transformer architecture with multi-head self-attention and causal attention masking. During inference, the model generates responses autoregressively, while during training, it optimizes cross-entropy loss between predicted and ground-truth tokens.

3.1.6. Hybrid Parameter Training Strategy

We employ a hybrid parameter optimization strategy that combines parameter-efficient LoRA adaptation for pre-trained components with full fine-tuning for novel architectural elements. Our trainable parameters consist of:

$$\Theta = \Delta\theta_{\text{LLM}} + \Delta\theta_{E_V} + \theta_{E_P} + \mathbf{sep}_{\text{grid}} + \mathbf{sep}_{\text{frame}} \quad (20)$$

where LoRA adapters are applied to the large language model ($\Delta\theta_{\text{LLM}}$) and visual encoder ($\Delta\theta_{E_V}$), while the multi-modal projector parameters (θ_{E_P}) and learnable separator tokens ($\{\mathbf{sep}_{\text{grid}}, \mathbf{sep}_{\text{frame}}\}$) are fully parameterized. Specifically, the frozen LLM backbone $\theta_{\text{LLM}}^{(0)}$ is augmented with low-rank adapters $\Delta\theta_{\text{LLM}} = \mathbf{A}\mathbf{B}$ where $\mathbf{A} \in \mathbb{R}^{d \times r}$ and $\mathbf{B} \in \mathbb{R}^{r \times d}$ with $r \ll d$ and d being the model's hidden dimension, and similarly for the visual encoder $\theta_{E_V}^{(0)} + \Delta\theta_{E_V}$. The multi-modal projector requires full optimization to establish effective cross-modal alignment, while the learnable separators $\mathbf{sep}_{\text{grid}}$ and $\mathbf{sep}_{\text{frame}}$ are trained from random initialization to capture surgical workflow dynamics. Following an instruction-tuning paradigm on dataset $\mathcal{D} = \{(\mathbf{I}_i, \mathbf{y}_i)\}_{i=1}^N$, where \mathbf{I}_i comprises video \mathbf{X} and question \mathbf{Q}_{ues} , and \mathbf{y}_i represents the ground-truth answer sequence $\mathbf{y}_i = \{y_{i,1}, y_{i,2}, \dots, y_{i,L_i}\}$ of length L_i , we optimize the cross-entropy loss function:

$$\mathcal{L}(\Theta) = - \sum_{i=1}^N \sum_{j=1}^{L_i} \log p_{\Theta}(y_{i,j} | \mathbf{I}_i, y_{i,<j}) \quad (21)$$

where $y_{i,<j} = \{y_{i,1}, \dots, y_{i,j-1}\}$ represents the preceding token sequence for autoregressive generation, and $p_{\Theta}(y_{i,j} | \mathbf{I}_i, y_{i,<j})$ denotes the probability of generating the correct token $y_{i,j}$ given the multimodal input \mathbf{I}_i and previous tokens, computed through the softmax-normalized output logits of F_{LLM} .

3.1.7. Surgical Competency Progression (SCP)

To address the inherent hierarchical dependency structure in surgical intraoperative assessments, where complex analytical tasks rely on fundamental surgical scene understanding capabilities, we design a Surgical Competency Progression (SCP) training scheme that mirrors the natural progression of surgical expertise acquisition. Our approach organizes training into three sequential stages aligned with the hierarchical task taxonomy: Perception, Assessment, and Reasoning.

Stage-wise Task Organization: We partition the dataset \mathcal{D} into three task-level subsets corresponding to the hierarchical levels:

- **Stage 1 (Perception):** $\mathcal{D}_P = \{\mathcal{D}_{\text{TP}}, \mathcal{D}_{\text{AP}}, \mathcal{D}_{\text{ASP}}\}$, encompassing fundamental surgical scene understanding tasks including tool perception, action perception, and anatomical structure perception.
- **Stage 2 (Assessment):** $\mathcal{D}_A = \{\mathcal{D}_{\text{CVSA}}, \mathcal{D}_{\text{DFA}}, \mathcal{D}_{\text{AEA}}, \mathcal{D}_{\text{SPA}}\}$, incorporating intraoperative assessment tasks including CVS evaluation, difficulty findings assessment, adverse events assessment, and surgical skill proficiency evaluation.
- **Stage 3 (Reasoning):** $\mathcal{D}_R = \{\mathcal{D}_{\text{SSD}}, \mathcal{D}_{\text{ARR}}, \mathcal{D}_{\text{CA}}, \mathcal{D}_{\text{IP}}\}$, comprising higher-order reasoning tasks including surgical scene description, action rationale reasoning, comprehensive assessment, and intra-operative planning.

Cumulative Training with Progressive Sampling: Our SCP follows a cumulative training paradigm where tasks from previous stages are retained in subsequent stages, ensuring that foundational capabilities are maintained while more complex reasoning skills are developed. To balance computational efficiency with knowledge retention, we employ a progressive sampling strategy that reduces the sampling rate of earlier-stage

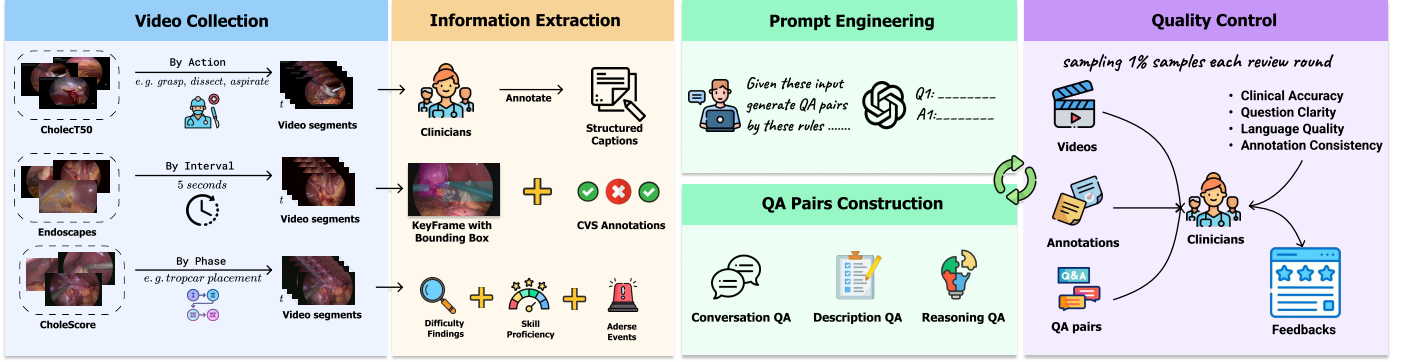


Fig. 4: Curation pipeline of the proposed dataset CholeVidQA-32K.

data as training advances. Specifically, at stage k , the effective training set is constructed as:

$$\mathcal{D}_{\text{eff}}^{(k)} = \bigcup_{j=1}^k \lambda_{k,j} \cdot \mathcal{D}_j \quad (22)$$

where \mathcal{D}_j represents the task subset at stage j , and $\lambda_{k,j} \in (0, 1]$ denotes the sampling rate for stage j data when training at stage k . We set $\lambda_{k,k} = 1.0$ to fully utilize current-stage tasks, while applying reduced sampling rates $\lambda_{k,j} < 1.0$ for $j < k$ to maintain earlier capabilities without overwhelming the training distribution. This formulation ensures that the model progressively builds upon foundational skills while adapting to increasingly complex analytical requirements.

Each stage is trained for one complete epoch over its effective dataset $\mathcal{D}_{\text{eff}}^{(k)}$, allowing the model to adequately internalize the task-specific patterns before progressing to the next complexity level. The stage-specific optimization objective is:

$$\mathcal{L}^{(k)}(\Theta) = - \sum_{(\mathbf{I}_i, \mathbf{y}_i) \in \mathcal{D}_{\text{eff}}^{(k)}} \sum_{j=1}^{L_i} \log p_{\Theta}(y_{i,j} | \mathbf{I}_i, y_{i,<j}) \quad (23)$$

The model parameters Θ are continuously updated across all three stages, with the final trained model encapsulating knowledge from the complete hierarchical training progression. To ensure fair comparison with baseline models, we constrain the sample size at each stage to match that of the baselines, thereby maintaining equivalence in the total number of training samples observed across all methods.

3.2. CholeVidQA-32K Dataset Curation

3.2.1. Overall Curation Pipeline

As illustrated in Figure 4, our dataset construction follows a systematic four-stage pipeline designed to ensure both scalability and clinical accuracy. The first stage encompasses video collection and segmentation, wherein surgical video clips are extracted from multiple sources and partitioned according to their distinct characteristics and annotation types. The second stage involves comprehensive information extraction, wherein diverse annotations—including temporal keyframes, binary classification labels, continuous scoring metrics, spatial bounding boxes, and expert-generated textual captions—are systematically aggregated, processed, and standardized into a unified format. In the third stage, we employ carefully engineered prompts to guide GPT-5.1 in generating open-ended question-answer pairs from the extracted multimodal annotations. To address

potential hallucination artifacts in large language model generation, we implement a stratified sampling protocol across each VQA category, resulting in 1% of the dataset (320 QA pairs), and engage one clinical expert in a structured review process to assess the generated content across four critical dimensions: (1) *Clinical Accuracy*, verifying factual correctness of medical terminology and procedural descriptions; (2) *Question Clarity*, confirming questions are unambiguous and clinically meaningful; (3) *Language Quality*, evaluating linguistic coherence and appropriate use of medical terminology; and (4) *Annotation Consistency*, checking alignment with existing clinical annotations and assessment frameworks. Expert feedback identifying deficiencies across these dimensions is subsequently formalized into refinement prompts that guide iterative improvement of the generated QA-pairs. Finally, the fourth stage encompasses rigorous quality assurance, wherein all test set samples undergo manual verification to eliminate hallucinations and ensure clinical validity.

3.2.2. Detailed Curation Process

To construct a dataset with rich hierarchical semantics, we adapt data from multiple established sources and partition them into three distinct subsets, designated with the VQA suffix: CholecT50-Caption-VQA, Endoscopes-VQA, and CholeScore-VQA. As illustrated in Figure 4, the detailed curation process for each subset is described below:

CholecT50-Caption-VQA: We begin by leveraging videos from the publicly available CholecT50 dataset (Nwoye et al., 2022), which provides laparoscopic surgical videos annotated with action triplets at one-second intervals. Each temporal frame contains annotations indicating the presence or absence of specific action triplets, with multiple concurrent actions possible within individual frames. We segment videos based on action consistency, grouping consecutive frames where the same set of actions remains unchanged. Subsequently, we engage clinical experts to annotate each video segment following a structured annotation framework encompassing anatomical descriptions, tool dynamics, and surgical action rationales, yielding over 1,500 caption-clip pairs. Based on these rich textual descriptions, we employ GPT-5.1 to generate three distinct categories of question-answer pairs: (1) *Conversational QA*, which isolates specific informational aspects from the captions including tools, anatomy, and actions, yielding the *Tool Perception (TP)*, *Action Perception (AP)*, and *Anatomical Structure Perception (ASP)* tasks at the perception level; (2) *Descriptive QA*, which synthesizes multiple aspects to provide comprehensive

surgical scene elaboration, corresponding to the *Surgical Scene Description* (SSD) task; and (3) *Reasoning QA*, which poses questions conditioned on the rationale of current operative actions, corresponding to the *Action Rationale Reasoning* (ARR) task (e.g., “Why does the surgeon remain stationary during this phase rather than immediately performing dissection or manipulation?”). The detailed prompt engineering strategy for this subset is provided in Appendix [Appendix A.1](#).

Endoscopes-VQA: To incorporate Critical View of Safety (CVS)—one of the most critical surgical safety assessment protocols—we adapt the Endoscopes dataset ([Mascagni et al., 2025](#)), which comprises 201 laparoscopic cholecystectomy videos with systematically annotated frames featuring CVS labels and spatial bounding boxes delineating critical anatomical structures. Each frame annotation consists of binary labels corresponding to the three established CVS criteria: the Two Structure criterion, the Hepatocystic triangle criterion, and the Cystic plate criterion. Each criterion focuses on the clear visual identification and adequate dissection of specific anatomical landmarks essential for safe surgical practice. Our objective extends beyond binary CVS prediction to enable interpretable reasoning that justifies the assessment decisions. To accomplish this, we implement temporal segmentation using fixed 5-second intervals that align with the original CVS annotation frequency, selecting the central frame of each segment as the representative keyframe. We enhance these keyframes by overlaying the corresponding bounding box annotations to provide explicit visual guidance for anatomical structure localization. To ensure comprehensive understanding of CVS assessment rationale, we incorporate the complete CVS annotation guidelines into our generation prompts, enabling GPT-5.1 to deduce reasoning based on visual evidence from the annotated keyframes—including anatomical structure presence and spatial relationships—in conjunction with the detailed procedural guidelines that encompass various decision scenarios for CVS achievement assessment. This approach yields three comprehensive question-answer pairs corresponding to each CVS criterion, characterized by open-ended formulations. The detailed prompt engineering approach for this subset is provided in Appendix [Appendix A.2](#).

CholeScore-VQA: To encompass comprehensive intraoperative assessment dimensions beyond CVS, including intraoperative difficulty evaluation, adverse event detection, and skill assessment, we introduce the CholeScore-VQA subset comprising 100 laparoscopic cholecystectomy videos from the CholeScore dataset ([Sharma et al., 2025](#)). Based on the nature of the annotations being phase-focused, we implement phase-based temporal segmentation, dividing procedures according to the six established surgical phases (e.g., trocar placement, hepatocystic triangle dissection), with individual procedures typically spanning 1-2 hours and resulting in extended video segments ranging from minutes to tens of minutes in duration. This subset incorporates three distinct categories of annotations: (1) *Operative Difficulty Assessment*, integrating three established difficulty scoring systems—the Nassar, Sugrue, and Parkland Grading Scale (PGS)—consolidating their evaluation criteria into discrete clinical findings represented as binary labels indicating the presence or absence of specific conditions (e.g., visceral fat, dense adhesions); (2) *Intraoperative Adverse Events (IAE)*, employing the SEVERE classification system to systematically catalog adverse

events including thermal injury, bleeding, and mechanical complications, with each event categorized according to severity levels ranging from 3 to 5 gradations;

(3) *Skill Assessment*, incorporating the Objective Structured Assessment of Technical Skills (OSATS) framework, which provides structured evaluation of procedural competency in critical anatomical manipulations (e.g., gallbladder fossa dissection) and operative goal completion (e.g., access port placement), with scores reflecting varying levels of surgical proficiency.

This comprehensive annotation set yields over 80 distinct assessment labels distributed across 499 video clips, with each surgical phase featuring phase-specific annotation sets that capture the unique safety considerations and technical challenges inherent to that procedural stage.

Following the consolidation of these multi-dimensional annotations, we formulate the task as phase-level video question answering. For each video segment, we provide GPT-5.1 with the complete set of phase-specific annotation labels accompanied by detailed descriptions of each assessment criterion. Consistent with the CholecT50-Caption-VQA methodology, we generate three distinct categories of question-answer pairs: (1) *Conversational QA*, which isolates individual annotation labels to formulate targeted questions and derives clinical reasoning based on the provided label descriptions, yielding the *Difficulty Findings Assessment* (DFA), *Adverse Events Assessment* (AEA), and *Skills Proficiency Assessment* (SPA) tasks; (2) *Descriptive QA*, which synthesizes all available labels to generate comprehensive safety assessments that holistically evaluate the procedural segment, corresponding to the *Comprehensive Assessment* (CA) task; and (3) *Reasoning QA*, which poses hypothetical scenario-based questions by modifying specific clinical findings (e.g., “Given dense fibrotic adhesions, how should the surgeon optimize port placement?”), strictly conditioned on the clinical definitions of each finding—including how it affects LCOD severity and what further intraoperative interventions it may require—corresponding to the *Intraoperative Planning* (IP) task. This subset is didactic in nature, designed to build procedural reasoning rather than perform actual assessment, and is validated by checking whether model responses adhere to the original clinical descriptions. The detailed prompt engineering methodology for this subset is provided in Appendix [Appendix A.3](#).

The detailed statistics of the resulting dataset are provided in Table 2, and a thorough breakdown of the three hierarchies, along with further breakdowns of each hierarchy and temporal duration, can be found in Figure 6.

3.2.3. Golden Test Set Curation

To explore the alignment between our proposed model and real-world clinicians’ reasoning processes during operations, we extract a subset of samples from the assessment level and engage clinical experts to manually create answers based on given videos and questions. The resulting golden test set statistics are shown in Table 3.

4. Experiment

4.1. Evaluation Pipeline

Given the complex nature of surgical video question answering tasks that encompass both categorical intraoperative as-

Dataset Subset	#Videos	Avg Length (sec)	#Conv. QA	#Desc. QA	#Reas. QA	#Total QA	Avg WC Questions	Avg WC Answers	Tasks
CholecT50-Caption-VQA	1544	3 ± 4	9550	1544	7274	18368	14 ± 4	48 ± 45	TP, AP, ASP, SSD, ARR
Endoscapes-VQA	1812	5 ± 0	5436	-	-	5436	22 ± 7	54 ± 11	CVSA
CholeScore-VQA	499	711 ± 818	6405	1051	1051	8507	18 ± 9	64 ± 70	DFA, SPA, AEA, CA, IP
Total	3.9K	95 ± 378	21.4K	2.6K	8.3K	32.3K	17 ± 7	53 ± 50	-

Table 2: Comprehensive statistics of CholeVidQA-32K subsets covering number of videos, average video length, number of conversational (Conv.), descriptive (Desc.), and reasoning (Reas.) QA pairs, total QA pairs, and average word count (WC) for questions and answers, with corresponding task abbreviations (see Subsubsection 3.2.2).

	CVS	LCOD	IAE	Skill	Total
#QA Pairs	30	61	15	15	121
#Videos	10	3	6	6	25

Table 3: Statistics of the golden test set with expert-annotated answers across different assessment subtasks.

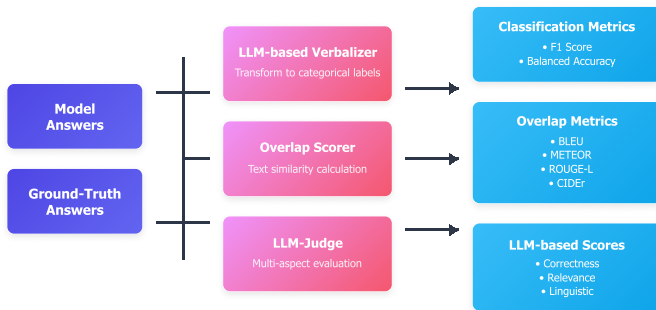


Fig. 5: Comprehensive evaluation pipeline for CholeVidQA-32K assessment framework incorporating three complementary evaluation methodologies for robust performance measurement.

assessments and open-ended clinical reasoning, we establish a comprehensive three-tier evaluation framework as illustrated in Figure 5. This multi-faceted approach addresses the inherent challenges in evaluating natural language responses for safety-critical surgical applications, where both factual accuracy and linguistic quality are paramount.

The evaluation pipeline processes model-generated answers and ground-truth answers through three distinct but complementary assessment streams: (1) **LLM-based Verbalizer** transforms both predicted and reference answers into standardized categorical labels, enabling systematic classification performance measurement through F1 scores (for DFA, SPA and AEA tasks) and balanced accuracy metrics (for CVSA task) that account for potential class imbalances inherent in clinical datasets. To reflect the model’s capability in providing evaluable results, we also report answer rate along with the scores. (2) **Overlap Scorer** conducts direct text similarity analysis between generated responses and reference responses using established natural language generation metrics including BLEU for n-gram precision, METEOR for semantic alignment with synonyms and paraphrases, ROUGE-L for longest common subsequence matching, and CIDEr for consensus-based evaluation that emphasizes clinically relevant terminology. (3) **LLM-Judge** performs sophisticated multi-aspect evaluation wherein large language models assess generated responses across three critical dimensions: correctness (clinical accuracy and factual

validity), relevance (appropriateness to the surgical context and question intent), and linguistic quality (coherence, clarity, and professional surgical terminology usage).

4.2. Dataset Split

We employ video-level stratified splitting strategies to ensure temporal independence and prevent data leakage across training, validation, and test sets. For **CholecT50-Caption-VQA**, we implement a 7:1:2 split ratio that balances training data sufficiency with robust evaluation set sizes. For **Endoscapes-VQA** and **CholeScore-VQA**, we adopt the original partitioning schemes from (Mascagni et al., 2025) and (Sharma et al., 2025) respectively to maintain consistency with prior assessment benchmarks. Table 4 summarizes the detailed statistics across all subsets.

Subset	#Videos			#QA Pairs		
	Train	Val	Test	Train	Val	Test
CholecT50-Caption-VQA	1.1K	155	309	12.9K	1.8K	3.7K
Endoscapes-VQA	1.2K	367	289	3.5K	1.1K	867
CholeScore-VQA	259	50	190	4.4K	860	3.2K

Table 4: Dataset split statistics across CholeVidQA-32K subsets.

4.3. Baseline Models

We evaluate the following zero-shot models on our dataset: mPLUG-Owl3 (Ye et al., 2024), InternVideo2.5 (Wang et al., 2025b), LongVA (Zhang et al., 2024a), LLaVA-Video (Zhang et al., 2024b), and VideoGPT+ (Maaz et al., 2024a). To isolate the effectiveness of our proposed model and ensure fair comparison while avoiding confounding effects from domain adaptation, we fine-tune LLaVA-Video and VideoGPT+ on our CholeVidQA-32K dataset, creating the LLaVA-Video-ft and VideoGPT+-ft baselines.

For all zero-shot models, we standardize the input to 64 uniformly sampled frames per video to ensure consistent temporal coverage and fair comparison. For fine-tuned models, memory constraints necessitate different configurations: LLaVA-Video-ft and VideoGPT+-ft processes 10 frames per video during training, and 64 frames are fed into the model during inference. Our proposed SurgTEMP leverages the TEMP module’s text-guided attention mechanism to achieve efficient visual token reduction, enabling processing of 64 frames during both training and inference stage. To ensure fair comparison in terms of computational cost, we configure the TEMP module to select top 10 frames equivalent in quantity to those processed by

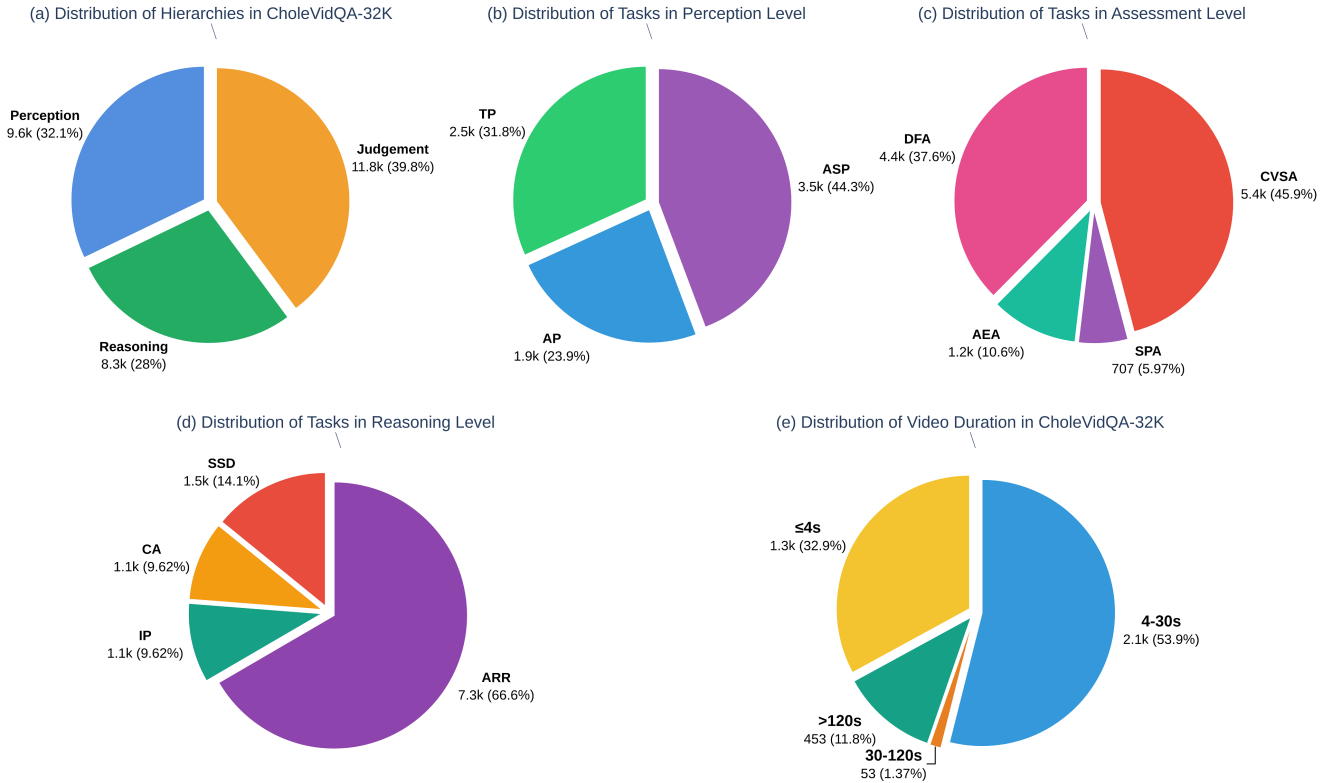


Fig. 6: Breakdown of CholeVidQA-32K composition and characteristics across hierarchy, tasks, and temporal duration. Task abbreviations: TP (Tool Perception), AP (Action Perception), ASP (Anatomical Structure Perception), CVSA (Critical View of Safety Assessment), DFA (Difficulty Findings Assessment), AEA (Adverse Events Assessment), SPA (Skills Proficiency Assessment), SSD (Surgical Scene Description), ARR (Action Rationale Reasoning), CA (Comprehensive Assessment), and IP (Intraoperative Planning).

LLaVA-Video-ft and VideoGPT+-ft, thereby maintaining comparable model complexity while demonstrating the benefits of denser temporal sampling followed by adaptive frame selection.

4.4. Implementation Details

We conduct all experiments on a dual-node infrastructure, each node equipped with NVIDIA A100 80GB GPUs. For SurgTEMP, we adopt the SigLIP ViT-SO400M/14-384 as the vision encoder, Qwen2-7B-Instruct as the LLM backbone, and the pretrained projector from Zhang *et al.* (2024b). We follow the image preprocessing pipeline from (Zhai *et al.*, 2023), resizing input frames to 384×384 pixels and applying normalization using ImageNet statistics. For spatial pooling after image encoding and cross-modal projection, we employ a bilinear pooling strategy with a stride of 2.

To ensure a fair comparison of learnable parameter budgets, we apply a consistent LoRA configuration of $r = 64$ and $\alpha = 16$ across all fine-tuned models. We employ a discriminative learning rate strategy: the vision encoder is updated with a learning rate of 2×10^{-6} , while all other trainable parameters use 1×10^{-5} . Training uses a cosine annealing scheduler with linear warmup over 3% of total training steps, with mixed-precision training using bfloat16 (bf16) for model weights and TensorFlow-32 (tf32) for matrix multiplications. All models are trained for 1 epoch on the combined training set with an effective batch size of 4 via gradient accumulation, requiring approximately 20 hours for SurgTEMP convergence. To ensure deterministic and reproducible results, we set temperature to 0 and employ greedy decoding for all model answer generation.

For evaluation, we use the open-source gpt-oss-120b (OpenAI *et al.*, 2025) as the LLM judge and verbalizer. To avoid potential judge bias on specific styles, we conduct exploration on multiple judge models: proprietary models including gpt-5.1 and gemini-2.5-pro, and open-source models including gpt-oss-120b (OpenAI *et al.*, 2025), Mixtral-8x7B-Instruct (Jiang *et al.*, 2024), and DeepSeek-V3 (DeepSeek-AI, 2024). With fixed evaluation settings including evaluated samples (the test set), scoring prompt, and evaluation criteria, we report their agreement on model performance ranking across each hierarchy of the dataset as shown in Table 5. Notably, our model is ranked first overall across all judge models.

Table 5: Kendall’s W coefficient across different judge models showing strong agreement on evaluated models’ ranking overall and within each hierarchy on our dataset.

Overall	Perception	Assessment	Reasoning
0.852	0.811	0.864	0.782

4.5. Results Analysis

4.5.1. Overall Performance and Domain Adaptation

Table 6 presents the averaged performance across all subsets, evaluated using three complementary metric categories: GPT-based scores, overlap metrics, and classification metrics.

Among open-source zero-shot models, VideoGPT+ emerges as the strongest baseline, achieving 36.65% correctness—a 3.36

Models	GPT Scores			Overlap Metrics				Classification Metrics			
	CR	RL	LG	BLEU	METEOR	ROUGE-L	CIDEr	bAcc		F1-score	
								Score	Rate	Score	Rate
<i>Open-source Zero-shot</i>											
mPLUG-Owl3	32.06	45.00	43.09	5.57	23.81	23.12	6.40	32.29	95	15.00	97
InternVideo2.5	16.28	19.38	16.56	2.93	8.87	9.78	4.67	25.71	91	1.24	7
LongVA	25.81	34.90	34.68	1.91	21.61	14.21	0.61	5.07	9	22.46	56
LLaVA-Video	33.29	41.07	38.72	3.76	21.39	17.20	4.01	27.34	49	12.56	65
VideoGPT+	36.65	48.32	46.61	3.83	21.96	22.68	14.19	40.2	68	25.13	78
<i>Fine-tuned</i>											
VideoGPT+-ft	64.06	73.58	71.63	14.62	33.29	31.87	42.33	52.37	95	49.3	82
LLaVA-Video-ft	60.05	67.30	65.56	14.67	32.44	31.41	40.85	51.31	88	44.2	63
ours	71.62	81.65	79.12	15.29	36.28	34.90	42.53	56.53	100	52.33	91

Table 6: Overall performance comparison of baseline models and our proposed method on the CholeVidQA-32K dataset. Models are grouped into Open-source Zero-shot and Fine-tuned categories. Metrics are grouped into GPT Scores (CR: Correctness, RL: Relevance, LG: Linguistic Quality), Overlap Metrics (BLEU, METEOR, ROUGE-L, CIDEr), and Classification Metrics (bAcc: balanced Accuracy, F1: F1-score). For classification metrics, Score represents the metric value and Rate represents the answer rate (%). Blue shading indicates best performance among open-source zero-shot models; red shading indicates best performance among fine-tuned models.

Models	CholecT50-Caption-VQA			Endoscapes-VQA			CholeScore-VQA		
	CR	RL	LG	CR	RL	LG	CR	RL	LG
<i>Open-source Zero-shot</i>									
mPLUG-Owl3	46.31	54.35	47.78	29.18	42.48	45.04	20.70	38.18	36.46
InternVideo2.5	12.47	14.30	12.56	34.50	41.13	34.82	1.88	2.72	2.31
LongVA	47.79	55.58	51.81	5.00	9.95	13.75	24.64	39.16	38.49
LLaVA-Video	50.77	56.72	52.34	30.27	41.98	41.61	18.82	24.52	22.22
VideoGPT+	46.04	53.69	46.66	38.79	50.47	53.94	25.11	40.79	39.23
<i>Fine-tuned</i>									
VideoGPT+-ft	72.53	77.55	74.59	71.32	86.65	88.39	48.34	56.54	51.91
LLaVA-Video-ft	71.66	76.17	72.56	66.24	78.73	79.73	42.24	47.00	44.38
ours	74.82	81.3	78.80	73.77	89.33	90.32	66.28	74.32	68.23

Table 7: GPT Score performance breakdown across the three CholeVidQA-32K subsets: CholecT50-Caption-VQA, Endoscapes-VQA, and CholeScore-VQA. All metrics are GPT-based evaluations with CR: Correctness, RL: Relevance, LG: Linguistic Quality. Blue shading indicates best performance among open-source zero-shot models; red shading indicates best performance among fine-tuned models.

Models	CholecT50-Caption-VQA				Endoscapes-VQA				CholeScore-VQA			
	BLEU	METEOR	ROUGE-L	CIDEr	BLEU	METEOR	ROUGE-L	CIDEr	BLEU	METEOR	ROUGE-L	CIDEr
<i>Open-source Zero-shot</i>												
mPLUG-Owl3	3.60	26.59	23.26	8.63	12.88	30.47	31.21	8.42	0.23	14.37	14.90	2.14
InternVideo2.5	1.72	7.15	7.17	10.78	7.05	18.78	21.50	3.10	0.01	0.67	0.66	0.12
LongVA	1.57	27.15	15.82	0.26	3.98	19.01	16.11	1.44	0.17	18.66	10.70	0.14
LLaVA-Video	3.02	26.27	20.77	8.40	8.06	27.69	22.68	3.17	0.19	10.22	8.15	0.45
VideoGPT+	4.81	27.12	27.18	21.50	12.92	29.59	33.37	9.29	0.27	14.01	14.68	2.18
<i>Fine-tuned</i>												
VideoGPT+-ft	15.87	39.33	38.2	77.14	24.66	42.33	41.28	34.58	3.33	18.22	16.12	15.27
LLaVA-Video-ft	15.97	39.20	37.99	76.94	24.44	41.83	41.06	33.23	3.59	16.28	15.19	12.38
ours	16.12	40.22	38.45	77.33	25.62	45.68	44.62	34.93	4.12	22.94	21.62	15.33

Table 8: Overlap Metrics performance breakdown across the three CholeVidQA-32K subsets: CholecT50-Caption-VQA, Endoscapes-VQA, and CholeScore-VQA. All metrics measure text similarity between generated and reference answers. Blue shading indicates best performance among open-source zero-shot models; red shading indicates best performance among fine-tuned models.

percentage point margin over the second-best LLaVA-Video (33.29%).

For classification metrics, mPLUG-Owl3 has relatively higher answer rates (with 95% for bAcc, and 97% for F1 score), yet struggles to produce accurate predictions. This discrepancy underscores the difficulty of surgical assessment tasks, including CVS criterion evaluation, difficulty findings, adverse event detection, and skill scoring, where high answer rates do not guarantee clinical validity. The gap between answer rate and accuracy reveals that zero-shot models often generate responses that superficially appear valid but fail to correctly apply domain-specific assessment frameworks.

For fine-tuned models, our SurgTEMP substantially outperforms both the LLaVA-Video-ft and VideoGPT+-ft baselines across all three GPT-based dimensions and all overlap metrics. Notably, our model achieves high answer rates for classification metrics, indicating that the model generates more accurate and confident responses.

4.5.2. Subset-Specific Performance Patterns

Tables 7 and 8 reveal model performance across our three complementary subsets, with each subset presenting distinct challenges that expose different model capabilities.

CholecT50-Caption-VQA Analysis: For this subset, several zero-shot models demonstrate reasonable transferability to surgical domain perception. LLaVA-Video and LongVA achieve 50.77% and 47.79% correctness respectively, with relevance scores of 56.72% and 55.58%, suggesting that their pre-training on general-domain video data provides some foundational capabilities for surgical scene understanding. In contrast, InternVideo2.5 achieves substantially lower scores (12.47% correctness, 14.30% relevance), with consistency across all three GPT metrics indicating systematic limitations likely stemming from domain distribution discrepancies in its training corpus.

SurgTEMP achieves better performance over the strongest fine-tuned baseline VideoGPT+-ft on this subset: +2.29 percentage points in correctness, +3.75 in relevance, and +4.21 in linguistic quality. For overlap metrics on CholecT50-Caption-VQA (Table 8), the trends largely mirror GPT-based evaluations.

Endoscapes-VQA Analysis: Our model demonstrates substantial improvements on this subset, with significant margins over the strongest fine-tuned baseline VideoGPT+-ft: +2.45 percentage points in correctness, +2.68 in relevance, and +1.93 in linguistic quality. The overlap metrics (Table 8) reflect similar trends; while these margins are less dramatic than GPT-based metrics, they demonstrate improved semantic alignment with reference answers.

The performance gap between fine-tuned and zero-shot models is pronounced on Endoscapes-VQA. Even the best-performing zero-shot model (VideoGPT+) achieves only 38.79% correctness, representing a 34.98 percentage point deficit compared to our model. This substantial discrepancy demonstrates that CVS assessment is a highly nuanced task requiring specialized domain expertise: models must understand not only anatomical structures but also the specific evaluation criteria defined in clinical guidelines, which cannot be acquired through general-domain pre-training alone.

CholeScore-VQA Analysis: This subset presents the most challenging evaluation scenario due to its variable task com-

plexity and extended temporal context (average 710 seconds). Zero-shot models struggle severely: InternVideo2.5 achieves only 1.88% correctness while the best-performing zero-shot model (VideoGPT+) reaches merely 25.11% correctness. After domain fine-tuning, VideoGPT+-ft demonstrates substantial improvement, reaching 48.34% correctness—representing a gain of over 23 percentage points compared to the best zero-shot baseline.

Our SurgTEMP achieves further improvements over VideoGPT+-ft: +17.94 percentage points in correctness, +17.78 in relevance, and +16.32 in linguistic quality. These substantial margins validate our architectural design motivation: long-range video understanding for comprehensive evaluation requires sophisticated temporal context aggregation mechanisms that can identify and retain information across extended temporal sequences. The overlap metrics on CholeScore-VQA (Table 8) also exhibit a clear margin between our model and all baselines.

4.5.3. Task Hierarchy Performance Analysis

To provide deeper insights into model capabilities across different clinical complexity levels, we analyze performance on the three-tiered task hierarchy proposed in our dataset design: *Perception*, *Assessment*, and *Reasoning*. Figure 7 visualizes the averaged performance across Correctness, Relevance, and Linguistic Quality metrics for each task category, revealing distinct performance patterns that highlight the unique challenges of surgical assessment.

Perception-Level Tasks: Among zero-shot models, LLaVA-Video demonstrates the strongest performance on all three tasks, with LongVA and mPLUG coming in second place with decent action perception recognition capability. VideoGPT+ shows comparatively weaker perception, suggesting its strengths lie more in assessment-level understanding. Both fine-tuned baselines, LLaVA-Video-ft and VideoGPT+-ft, achieve substantial improvements over their zero-shot counterparts, validating that surgical domain exposure enables better recognition of specialized instruments, anatomical structures, and procedural actions. Our SurgTEMP on these three tasks shows modest margins over both fine-tuned baselines on action and tool recognition while showing a decent margin on anatomical structures.

Assessment-Level Tasks: This hierarchy represents a more challenging and expertise-demanding category, where most zero-shot models struggle significantly. After domain fine-tuning, both LLaVA-Video-ft and VideoGPT+-ft achieve substantial improvements. Our SurgTEMP demonstrates the most improvement on this hierarchy, achieving 69.77% average correctness, which shows a notable margin over both fine-tuned baselines. This substantial gain validates our architectural design hypothesis: the TEMP module's text-guided memory construction mechanism enables targeted attention to assessment-related visual cues (e.g. anatomical landmarks for CVS assessment, surgical maneuvers for skill evaluation, abnormal tissue appearances for adverse event detection) that are essential for accurate clinical assessment.

Examining individual tasks, CVSA shows the greatest benefit from domain adaptation, in which zero-shot models achieve less than 40% correctness, yet after fine-tuning, performance boosts to over 70%. For difficulty findings and skill proficiency assessments, our model shows significant margins over all base-

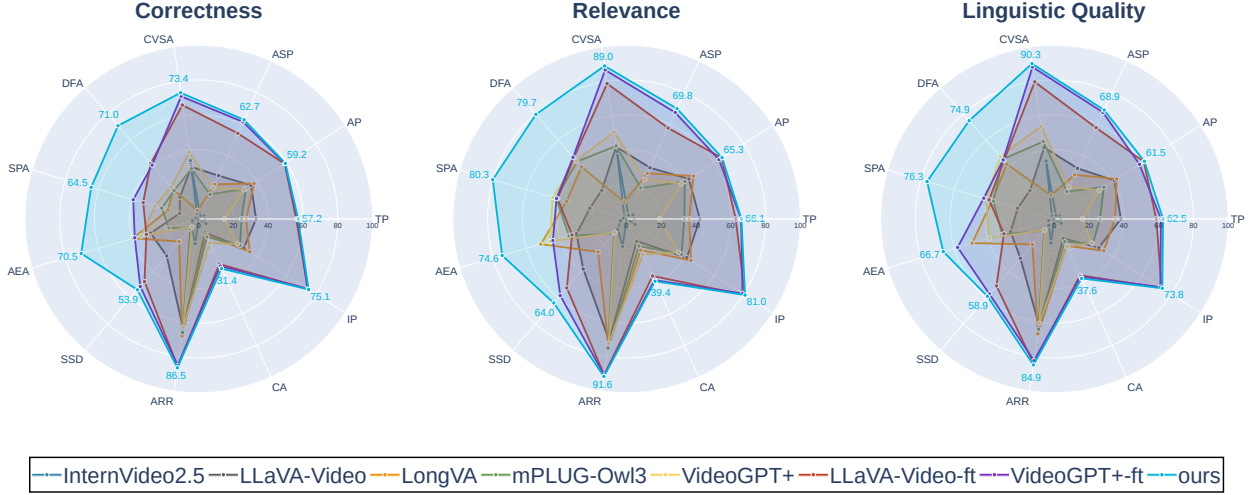


Fig. 7: Performance comparison across task hierarchies and granular task categories. The radar chart visualizes model performance on three hierarchical levels: **Perception** (basic surgical scene understanding including tool [TP], action [AP], and anatomical structure recognition [ASP]), **Assessment** (safety-focused assessments including CVS criteria [CVSA], difficulty findings [DFA], skill proficiency [SPA], and adverse events [AEA]), and **Reasoning** (surgical scene description [SSD], action rationale reasoning [ARR], comprehensive assessment [CA] and intraoperative planing [IP]). Results are averaged across Correctness, Relevance, and Linguistic Quality metrics. Our SurgTEMP demonstrates balanced excellence across all hierarchy levels.

lines, which represents the critical need for adaptive attention allocation on temporal span. For adverse event detection, even the fine-tuned baseline cannot achieve reasonably good performance. We hypothesize this is because adverse events rely on detecting fine-grained and sudden status changes of anatomical structures.

Reasoning-Level Tasks: This hierarchy encompasses the most cognitively complex tasks requiring synthesis of multiple information sources. For descriptive tasks SSD and CA, which rely on surgical scene understanding and intraoperative assessment capabilities, zero-shot models fall short. After fine-tuning, both LLaVA-Video-ft and VideoGPT+-ft achieve substantial improvements, and our model achieves a visible margin over both. For the action rationale task, which requires more basic domain understanding including the maneuvers and intent of operative actions, general domain knowledge transfer works better for zero-shot models, and after fine-tuning, the gains remain positive. Yet for the intraoperative planning task that requires contextual analysis and understanding of potential risk management expertise, zero-shot models struggle, with performance mostly below 30% correctness.

4.5.4. Ablation Study

To validate the individual contributions of our proposed architectural components and strategy, we conduct a systematic ablation study by progressively removing key modules from SurgTEMP. Table 9 presents the averaged performance across all three CholeVidQA-32K subsets.

Temporal Memory Bank (TMB): Removing the hierarchical temporal memory pyramid construction (ours w/o TMB) results in performance degradation of 5.81, 5.86, and 6.51 percentage points in correctness, relevance, and linguistic quality respectively compared to the full model. This substantial drop validates the importance of the temporal memory bank, which provides a proxy for coarse long-range observation aggregation for surgical video understanding.

Text-guided Attention Selection (TAS): Disabling the text-guided visual token selection mechanism, which we replace the

Models	Components					GPT Scores		
	VI	TMB	TAS	LS	SCP	CR	RL	LG
w/o TMB	✓	✗	✓	✓	✓	66.6	76.34	73.56
w/o TAS	✓	✓	✗	✓	✓	64.19	71.48	69.02
w/o LS	✓	✓	✓	✗	✓	67.01	76.3	74.13
w/o SCP	✓	✓	✓	✓	✗	69.73	80.2	78.39
w/o VI	✗	✓	✓	✓	✓	8.12	10.70	9.38
Full Model	✓	✓	✓	✓	✓	71.74	81.73	79.35

Table 9: Ablation study evaluating the contribution of each architectural component. VI: Visual Input, TMB: Temporal Memory Bank, TAS: Text-guided Attention Selection, LS: Learnable Separator, SCP: Surgical Competency Progression. ✓ indicates component present, ✗ indicates component removed. GPT Scores: Correctness (CR), Relevance (RL), Linguistic Quality (LG).

attention-based top- k frame selection with a randomized one, (ours w/o TAS) causes a notable performance drop: correctness drops by 7.55 points, relevance by 10.25 points, and linguistic quality by 10.33 points. This degradation demonstrates that the TAS module’s ability to dynamically prioritize surgical task-relevant visual clues.

Learnable Separator (LS): Replacing the learnable separator tokens with fixed all-zero vectors (ours w/o LS) results in performance degradation of 4.73 points in correctness, 5.43 points in relevance, and 5.22 points in linguistic quality. This consistent drop validates that learnable separators, compared to simple zero-vector separators, provide more meaningful structural boundaries that guide hierarchical memory organization. Without content-aware learned separators to demarcate temporal hierarchy levels, the model’s ability to maintain coherent spatial-temporal relationships across the memory pyramid is weakened, reducing precision in both spatial and temporal reasoning.

Surgical Competency Progression (SCP): Removing the SCP training scheme (ours w/o SCP) results in moderate performance degradation of 2.01 points in correctness, 1.53 points in relevance, and 0.96 points in linguistic quality. While the per-

formance drop is less severe than removing architectural components, these decreases demonstrate the importance of our progressive training approach that gradually introduces tasks of increasing complexity. The SCP training scheme enables more robust feature representations by first establishing strong perceptual foundations before building higher-level clinical reasoning capabilities.

Component Synergy: The ablation results reveal that all components and training strategies contribute substantially and complementarily to model performance. The cumulative performance gap between the worst ablation (ours w/o TAS: 64.19% CR) and the full model (71.74% CR) reaches 7.55 percentage points, demonstrating that our architectural innovations provide meaningful improvements over baseline temporal fusion approaches.

Visual Inputs (VI): To validate that the model does not shortcut by relying solely on textual questions to produce answers, we remove all visual inputs. The dramatic performance collapse confirms both the validity of the dataset generation pipeline and the effectiveness of the model in leveraging visual signals rather than overfitting on textual associations between questions and answers.

4.5.5. Parameters Sensitivity Analysis

Frame Sampling Upperbound Analysis: To validate the temporal scaling behavior of our TEMP module, we conduct systematic experiments varying the number of uniformly sampled frames from 16 to 96. As illustrated in Figure 8a, model performance exhibits a clear non-monotonic relationship with temporal sampling density across all three subsets. During the initial scaling phase (16 to 64 frames), correctness consistently improves across all subsets as increased temporal coverage enables better understanding of surgical context and procedural progression. However, the rate of improvement varies significantly between subsets. CholecT50-Caption-VQA exhibits early performance saturation, plateauing around 32 frames with marginal gains thereafter (75.17% at 32 frames vs. 74.73% at 80 frames). This early plateau indicates that the subset’s relatively short video segments and straightforward question types require limited long-range temporal dependencies, making dense sampling beyond 32 frames unnecessary for this particular task distribution. In contrast, Endoscapes-VQA and CholeScore-VQA demonstrate sustained performance improvements throughout the scaling range, reaching peak performance at 64-80 frames. Endoscapes-VQA achieves 73.40% correctness at 64 frames compared to 61.25% at 16 frames (+12.15%), while CholeScore-VQA shows even more dramatic gains: 66.88% at 80 frames versus 57.47% at 16 frames (+9.41%). These substantial improvements validate that intraoperative assessment tasks—particularly CVS evaluation requiring fine-grained anatomical detail and skill proficiency assessment requiring comprehensive temporal context—benefit significantly from denser temporal sampling and the TEMP module’s hierarchical memory construction mechanism.

Beyond the optimal operating point at 64 frames, all subsets experience performance degradation at 96 frames, with correctness dropping dramatically: CholecT50-Caption-VQA falls to 53.74% (-21.51 points from 80 frames), Endoscapes-VQA to 59.71% (-12.35 points), and CholeScore-VQA to 52.72% (-14.16 points). We hypothesize this degradation stems from two compounding factors: (1) **information saturation**, where

excessive temporal sampling introduces redundant visual content that dilutes attention to critical frames, and (2) **capacity limitations** of the TEMP module’s top- k selection mechanism, which struggles to effectively filter salient information from an overwhelming pool of 96-frame candidates, leading to suboptimal token selection and reduced reasoning quality. These findings establish 64 frames as the optimal configuration for our architecture, achieving the best trade-off between comprehensive temporal coverage and efficient information extraction.

Frame Selection Temperature Parameter Analysis: Complementing the frame sampling analysis, we investigate the sensitivity of our TEMP module to the Gumbel-Softmax temperature parameter σ , which controls the sharpness of differentiable frame selection. As shown in Figure 8b, the optimal temperature exhibits a clear inverted-U relationship with performance, with subset-specific peaks that reflect the underlying temporal structure of safety-critical information. Endoscapes-VQA achieves optimal performance at $\sigma = 0.05$ (73.46% correctness), demonstrating that Critical View of Safety assessment benefits from sharp, near-deterministic frame selection to precisely localize anatomical landmarks (cystic duct, cystic artery, hepatocystic triangle) within brief 5-second clips where critical structures appear in specific frames. This sharp selection enables the model to commit decisively to frames containing CVS-relevant anatomical features while filtering out transitional or irrelevant content.

In contrast, CholecT50-Caption-VQA and CholeScore-VQA reach optimal performance at $\sigma = 0.2$ (77.31% and 67.50% correctness respectively), indicating that skill assessment, operative difficulty evaluation, and adverse event detection require softer selection to integrate complementary visual evidence distributed across temporal sequences. The moderate temperature allows the model to maintain gradient flow during training while preserving sufficient selectivity to identify safety-critical patterns across extended procedural phases.

Performance degradation at extreme temperature values validates our architectural design choices. At $\sigma = 0.5$, excessive softness causes diffuse attention where selection becomes too uniform across frames, diluting safety-critical visual cues with irrelevant content—overall correctness drops to 65.86%, consistent with the information saturation observed at 96 frames. Conversely, excessively sharp selection ($\sigma = 0.05$) harms longer-context subsets by over-committing to specific frames during training, limiting gradient flow and reducing the model’s ability to discover diverse safety-critical patterns: CholecT50-Caption-VQA and CholeScore-VQA drop to 70.26% and 58.86% respectively. These findings establish $\sigma = 0.2$ as our default configuration, balancing differentiability for end-to-end training with sufficient selectivity for effective frame filtering, while demonstrating that the optimal operating point depends on video length characteristics and the spatial versus temporal distribution of task-relevant information within each subset.

4.5.6. Results Analysis on Golden Test Set

To validate the alignment between model-generated responses and real-world clinical reasoning processes, we construct a golden test set comprising 121 expert-annotated question-answer pairs spanning four assessment-level tasks. Unlike the main test set where ground-truth answers are derived from structured clinical annotations and repurposed by

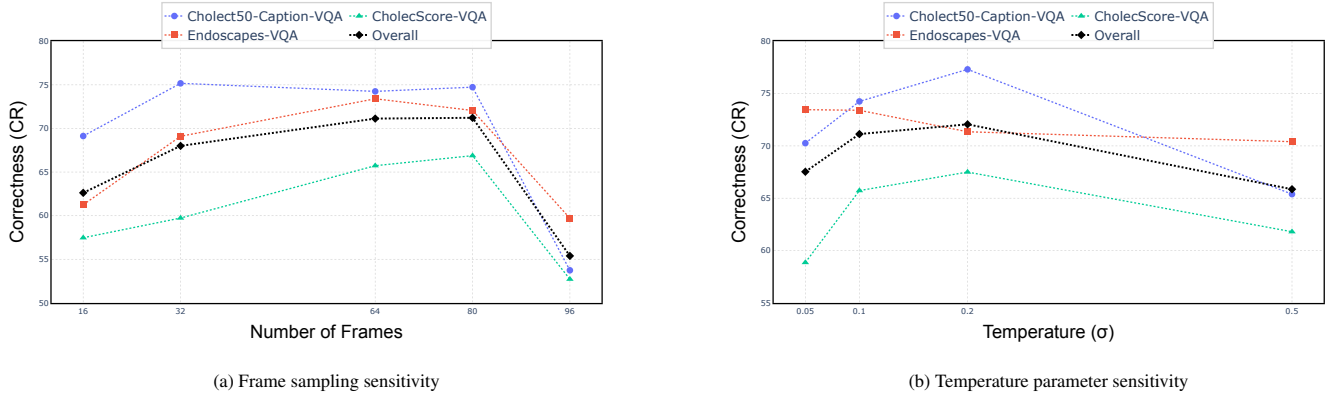


Fig. 8: Parameter sensitivity analysis of our TEMP module. (a) Impact of frame sampling rate: Correctness (CR) scores as a function of uniformly sampled frames (16, 32, 64, 80, 96). Performance improves with denser temporal sampling up to 64 frames, then degrades at 96 frames due to information saturation. (b) Impact of Gumbel-Softmax temperature (σ): CR scores across temperature values (0.05, 0.1, 0.2, 0.5). Optimal temperature exhibits subset-specific patterns, with Endoscapes-VQA benefiting from sharp selection ($\sigma = 0.05$) while longer-context subsets perform best with moderate softness ($\sigma = 0.2$).

LLM, this golden set features answers directly authored by clinical experts based on video content and surgical domain knowledge, providing a benchmark for evaluating models' capability to align with authentic clinical reasoning patterns. As presented in Table 10, our SurgTEMP consistently outperforms all baselines across both GPT-based and overlap metrics on this expert-curated evaluation set.

Examining individual task performance reveals distinct patterns reflecting varying assessment complexities. For CVSA, our model outperforms LLaVA-Video-ft by +6.84 points, representing the smallest margin among assessment tasks. In contrast, difficulty findings assessment (DFA) exhibits substantially larger gains (+24.05 points over VideoGPT+-ft), indicating that identifying operative difficulty factors (e.g., dense adhesions, visceral fat) demands more sophisticated visual pattern recognition and contextual interpretation that our TEMP module's text-guided attention mechanism effectively captures. The most dramatic performance gap emerges in adverse event assessment (AEA), where our model surpasses VideoGPT+-ft by +44.53 points. This substantial margin validates that detecting subtle tissue abnormalities, thermal injuries, and bleeding complications requires fine-grained temporal-spatial attention to transient visual cues that standard architectures often overlook. For skill proficiency assessment (SPA), our model achieves a +28.04-point margin over VideoGPT+-ft, confirming the importance of comprehensive temporal context integration for evaluating surgical technique quality across extended procedural phases. These results collectively demonstrate that our model's hierarchical memory construction and text-guided selection mechanisms enable closer alignment with expert clinical reasoning, particularly for tasks requiring detection of subtle safety-critical visual patterns and integration of long-range temporal dependencies.

4.5.7. Qualitative Results

To provide concrete insights into model behavior on each task, Figure 9, 10, 11 and 12 presents qualitative examples of model responses on all level questions. The examples demonstrate that our SurgTEMP generates responses that are not only factually correct but also clinically appropriate and linguistically coherent, while baseline models often produce responses that are either too generic, factually incorrect, or fail to apply

proper clinical assessment criteria.

4.6. Frame Selection Visualization

To showcase the effectiveness of the frame selection mechanism in our proposed TEMP module, we provide visualizations in Figures 13 and 14. In the first visualization (Figure 13), the model accurately selects the most informative frame as its top-2 selection and actively avoids out-of-body frames that are not helpful to the assessment. In the second visualization (Figure 14), the model selects the most informative frame as its top-7 selection, while also distributing attention to injury-relevant frames such as those showing bleeding and focusing on gallbladder bed dissection views.

5. Discussion

5.1. Limitations and Future Work

While our work establishes a comprehensive benchmark for safety-critical surgical VQA and demonstrates the effectiveness of the proposed SurgTEMP architecture, several limitations merit discussion and suggest promising directions for future research.

Dataset Scope and Procedural Coverage: Our CholeVidQA-32K dataset focuses exclusively on laparoscopic cholecystectomy, which, while being one of the most commonly performed minimally invasive procedures and featuring well-established safety assessment frameworks (CVS, difficulty grading systems, OSATS), limits the generalizability of our findings to other surgical specialties. Future work should extend the dataset to encompass diverse procedures such as colorectal surgery, bariatric surgery, and robotic-assisted interventions, each presenting unique anatomical challenges, instrument configurations, and safety considerations. Such expansion would enable investigation of cross-procedural transfer learning and development of procedure-agnostic safety assessment capabilities.

Handling Uncertainty and Abstention: Surgical decision-making inherently involves uncertainty, particularly in ambiguous scenarios where visual evidence may be insufficient for definitive safety assessment. While our model achieves high

Models	CVSA		DFA		AEA		SPA	
	GPT	Overlap	GPT	Overlap	GPT	Overlap	GPT	Overlap
<i>Open-source Zero-shot</i>								
mPLUG-OwI3	35.27	18.44	42.19	9.73	14.67	7.34	32.02	7.85
InternVideo2.5	40.61	10.99	3.22	0.57	6.44	0.39	0.00	0.00
LongVA	11.17	11.16	39.54	7.45	46.00	6.26	35.36	6.39
LLaVA-Video	45.16	15.34	14.18	6.56	20.22	3.19	21.43	4.81
VideoGPT+	46.93	18.81	43.96	9.80	12.44	7.46	32.50	6.82
<i>Fine-tuned</i>								
VideoGPT+-ft	80.24	29.33	42.13	13.2	23.16	8.35	52.77	11.82
LLaVA-Video-ft	81.30	29.76	38.46	13.74	17.11	5.53	48.29	12.30
ours	88.14	30.27	66.18	14.06	67.69	10.45	80.81	12.84

Table 10: Performance comparison between baselines and our model across tasks in the assessment hierarchy, including CVSA, DFA, AEA, and SPA, with two macro-averaged metrics. GPT indicates the averaged scores across all three dimensions: correctness, relevance, and linguistic quality. Overlap indicates the weighted average of BLEU, METEOR, ROUGE-L, and CIDEr that maps all metrics to a 0-100 scale.

answer rates (up to 100% for certain tasks), indiscriminate response generation without uncertainty quantification poses potential safety risks in clinical deployment. Future work should incorporate calibrated confidence estimation mechanisms that enable the model to appropriately abstain from answering when evidence is insufficient, provide confidence intervals for safety assessments, and identify scenarios requiring additional clinical expertise or alternative imaging modalities for verification.

5.2. Conclusion

This work addresses critical gaps in surgical data science by introducing both a comprehensive benchmark and a novel architectural solution for video question answering in laparoscopic cholecystectomy. We present CholeVidQA-32K, a hierarchical dataset encompassing 32K question-answer pairs across 11 distinct tasks organized into three levels of cognitive complexity—Perception (tool, action, and anatomical structure recognition), Assessment (Critical View of Safety, difficulty findings, adverse events, and skill proficiency evaluation), and Reasoning (surgical scene description, action rationale, comprehensive assessment, and intraoperative planning). Through systematic curation leveraging diverse annotation sources, our dataset establishes a foundation for developing and evaluating surgical VQA systems that extend beyond generic scene understanding.

To address the fundamental challenges of domain-specific visual interpretation, variable spatiotemporal granularity needs, and hierarchical task dependencies, we propose SurgTEMP with the Text-guided Memory Pyramid (TEMP) module. By utilizing textual queries as guiding signals for intelligent visual token selection through differentiable Gumbel-Softmax top- k frame selection and constructing hierarchical memory structures that balance fine-grained spatial details with long-term temporal context, our architecture directly tackles the knowledge-driven nature of surgical videos where anatomical structures often lack strong visual contrast. Furthermore, our Surgical Competency Progression (SCP) training scheme explicitly models task dependencies, progressively training the model from fundamental perception capabilities to higher-level assessment and reasoning tasks.

Comprehensive evaluation using three complementary metric tiers—GPT-based scores (correctness, relevance, linguistic quality), overlap metrics (BLEU, METEOR, ROUGE-

L, CIDEr), and classification metrics (balanced accuracy, F1-score)—reveals critical findings: while general-domain video MLLMs demonstrate reasonable zero-shot performance on basic perception tasks, their performance falls short on assessment-level tasks, underscoring the necessity of specialized domain adaptation and architectural solutions. Our SurgTEMP achieves substantial improvements over the baselines across all evaluation dimensions, with notable gains on assessment tasks and the long-context subset, validating that text-guided attention mechanisms and hierarchical temporal memory structures are essential for identifying and reasoning about subtle safety-critical visual cues across extended procedural contexts.

Acknowledgment

This work has received funding from the European Union (ERC, CompSURG, 101088553). Views and opinions expressed are however those of the authors only and do not necessarily reflect those of the European Union or the European Research Council. Neither the European Union nor the granting authority can be held responsible for them. This work was also partially supported by French state funds managed by the ANR under Grants ANR-10-IAHU-02 (IHU Strasbourg), ANR-23-IACL-0004 (AI Cluster Grand Est ENACT) and by the Interdisciplinary Thematic Institute HealthTech (ITI 2021-2028 program of the University of Strasbourg, CNRS and Inserm) via the IdEx Unistra (ANR-10-IDEX-0002) and SFRI (STRATUS project, ANR-20-SFRI-0012). This work was also granted access to the servers/HPC resources managed by CAMMA, IHU Strasbourg and Unistra Mesocentre.

References

- Agrawal, A., Lu, J., Antol, S., Mitchell, M., Zitnick, C.L., Batra, D., Parikh, D., 2016. Vqa: Visual question answering. URL: <https://arxiv.org/abs/1505.00468>, arXiv:1505.00468.
- Alapatt, D., Murali, A., Srivastav, V., Consortium, A., Mascagni, P., Padoy, N., 2024. Jumpstarting surgical computer vision, in: International Conference on Medical Image Computing and Computer-Assisted Intervention, Springer. pp. 328–338.
- Alayrac, J.B., Donahue, J., Luc, P., Miech, A., Barr, I., Hasson, Y., Lenc, K., Mensch, A., Millican, K., Reynolds, M., Ring, R., Rutherford, E., Cabi, S.,

Tool Perception [TP]	Action Perception [AP]	Anatomical Structure Perception [ASP]
<p>What instruments are in use, and how are they positioned?</p>  <p>0s 1s 3s</p>	<p>What action is the surgeon performing in this video?</p>  <p>0s 1s 2s</p>	<p>Can you describe the anatomical spaces visible in the video?</p>  <p>0s 2s 5s</p>
<p>Answer: There are three instruments: One grasper comes from the top side of the camera and is holding the distal side of the gallbladder. Another grasper comes from the left side of the camera and is retracting the proximal side of the gallbladder to the left. The hook comes from the right side of the camera and is approaching the cystic pedicle for dissection.</p>	<p>Answer: The surgeon intends to remove the gallbladder from the abdominal cavity using the specimen bag.</p>	<p>Answer: Absolutely. On the top side of the camera, we can see the abdominal cavity wall, which is yellow-pink with thin red blood vessels. The gallbladder and the cystic pedicle rest on the liver. The liver itself appears as a dark red structure with white granulations, spanning the right-center to left-center of the camera view. There's a porcelain gallbladder, a blue-green structure with thin red blood vessels, located at the center-left in front of the liver. On the distal side of the gallbladder, black grip marks made by a grasper are visible. The omentum, which is a rough yellow structure with red blood vessels, covers the duodenum at the bottom of the view. The duodenum can be seen as a pink structure on the bottom-right side, and the falciform ligament, which appears yellow-orange with thin red blood vessels, resides on the center-right side of the camera.</p>
<p>LLaVA-Video: The surgical instruments in use are a clamp and a hook. The clamp is positioned to hold the liver tissue steady, while the hook is used to manipulate or dissect the liver.</p>	<p>LLaVA-Video: The video shows a surgical procedure being performed on the gallbladder.</p>	<p>LLaVA-Video: The anatomical spaces visible in the video include the liver, which is a large organ located in the upper right quadrant of the abdomen. The liver is responsible for numerous vital functions such as detoxification, protein synthesis, and metabolism. In this particular view, we can see the liver's surface with its characteristic lobes structure, which is divided into right and left lobes. The video also shows parts of the surrounding tissues, including the peritoneum, which is a thin membrane that lines the abdominal cavity and covers the abdominal organs.</p>
<p>{'Correctness': 30, 'Relevance': 50, 'Linguistic': 25}</p>	<p>{'Correctness': 10, 'Relevance': 30, 'Linguistic': 40}</p>	<p>{'Correctness': 20, 'Relevance': 30, 'Linguistic': 40}</p>
<p>LLaVA-Video-ft: One grasper is visible on the left side of the camera, retracting the proximal gallbladder to the left. The hook instrument is coming from the right side of the camera and is being used to dissect the cystic pedicle.</p>	<p>LLaVA-Video-ft: The specimen bag is being closed by the surgeon.</p>	<p>LLaVA-Video-ft: The liver is a dark red structure with white granulations, located from the left-center to the right-center of the camera. The gallbladder and cystic pedicle are resting on it.</p>
<p>{'Correctness': 66, 'Relevance': 100, 'Linguistic': 90}</p>	<p>{'Correctness': 20, 'Relevance': 50, 'Linguistic': 70}</p>	<p>{'Correctness': 40, 'Relevance': 50, 'Linguistic': 70}</p>
<p>Ours: The grasper is coming from the left side of the camera and is grasping the proximal side of the gallbladder. Another grasper is on the top side of the camera. The hook is coming from the right side of the camera and is dissecting the cystic pedicle.</p>	<p>Ours: The surgeon is preparing to remove the gallbladder from the abdominal cavity using the specimen bag.</p>	<p>Ours: The liver is the smooth, dark-red structure extending from the right to the left side of the camera's view. The gallbladder is a pear-shaped, light-yellow structure located on the top-left side of the view, with visible red blood vessels. The cystic pedicle connects the gallbladder to the bottom-right of the view and appears dissected, showing some bleeding. The duodenum or intestine is seen as a pink structure at the bottom-right, covered by the yellow omentum.</p>
<p>{'Correctness': 85, 'Relevance': 100, 'Linguistic': 90}</p>	<p>{'Correctness': 100, 'Relevance': 100, 'Linguistic': 100}</p>	<p>{'Correctness': 70, 'Relevance': 80, 'Linguistic': 75}</p>

Fig. 9: Qualitative comparison of model responses on perception-level tasks, with key answer highlighted with red color font. The figure demonstrates how our SurgTEMP generates clinically accurate and contextually appropriate responses for tasks including tool perception, action perception, and anatomical structure perception, compared to baseline models.

- Han, T., Gong, Z., Samangoeei, S., Monteiro, M., Menick, J., Borgeaud, S., Brock, A., Nematzadeh, A., Sharifzadeh, S., Binkowski, M., Barreira, R., Vinyals, O., Zisserman, A., Simonyan, K., 2022. Flamingo: a visual language model for few-shot learning. URL: <https://arxiv.org/abs/2204.14198>, arXiv:2204.14198.
- Ali, S., Dmitrieva, M., Ghatwary, N., Bano, S., Polat, G., Temizel, A., Krenzer, A., Hekalo, A., Guo, Y.B., Matuszewski, B., Gridach, M., Voiculescu, I., Yoganand, V., Chavan, A., Raj, A., Nguyen, N.T., Tran, D.Q., Huynh, L.D., Boutry, N., Rezvy, S., Chen, H., Choi, Y.H., Subramanian, A., Balasubramanian, V., Gao, X.W., Hu, H., Liao, Y., Stoyanov, D., Daul, C., Realdon, S., Cannizzaro, R., Lamarque, D., Tran-Nguyen, T., Bailey, A., Braden, B., East, J.E., Rittscher, J., 2021. Deep learning for detection and segmentation of artefact and disease instances in gastrointestinal endoscopy. Medical Image Analysis 70, 102002. URL: <https://www.sciencedirect.com/science/article/pii/S1361841521000487>, doi:<https://doi.org/10.1016/j.media.2021.102002>.
- Allan, M., Shvets, A., Kurmann, T., Zhang, Z., Duggal, R., Su, Y.H., Rieke, N., Laina, I., Kalavakonda, N., Bodenstedt, S., et al., 2019. 2017 robotic instrument segmentation challenge. arXiv preprint arXiv:1902.06426.
- AYobi, N., Rodríguez, S., Pérez, A., Hernández, I., Aparicio, N., Dessevres, E., Peña, S., Santander, J., Caicedo, J.I., Fernández, N., Arbeláez, P., 2025. Pixel-wise recognition for holistic surgical scene understanding. Medical Image Analysis 106, 103726. URL: <https://www.sciencedirect.com/science/article/pii/S1361841525002737>, doi:<https://doi.org/10.1016/j.media.2025.103726>.
- Bai, J., Bai, S., Yang, S., Wang, S., Tan, S., Wang, P., Lin, J., Zhou, C., Zhou, J., 2023a. Qwen-vl: A versatile vision-language model for understanding, localization, text reading, and beyond. URL: <https://arxiv.org/abs/2308.12966>, arXiv:2308.12966.
- Bai, L., Islam, M., Seenivasan, L., Ren, H., 2023b. Surgical-vqla: Transformer with gated vision-language embedding for visual question localized-answering in robotic surgery, in: 2023 IEEE International Conference on Robotics and Automation (ICRA), IEEE, pp. 6859–6865.
- Bose, R., Nwoye, C.I., Lazo, J., Lavanchy, J.L., Padoy, N., 2025. Feature mixing approach for detecting intraoperative adverse events in laparoscopic roux-en-y gastric bypass surgery. URL: <https://arxiv.org/abs/2504.16749>, arXiv:2504.16749.
- Chen, X., Djolonga, J., Padlewski, P., Mustafa, B., Changpinyo, S., Wu, J., Ruiz, C.R., Goodman, S., Wang, X., Tay, Y., Shakeri, S., Dehghani, M., Salz, D., Lucic, M., Tschannen, M., Nagrani, A., Hu, H., Joshi, M.,

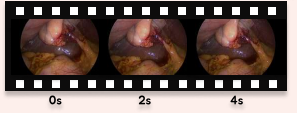
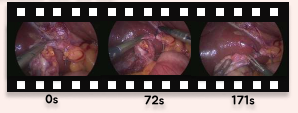
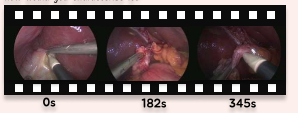

Critical View of Safety Assessment [CVSA]	Skill Proficiency Assessment [SPA]	Adverse Events Assessment [AEA]	Difficulty Findings Assessment [DFA]
<p>In this video, is the two-structure criterion achieved? Why?</p>  <p>0s 2s 4s</p>	<p>How would you rate the cystic duct clipping and division on a 2-10 performance scale, and why?</p>  <p>0s 72s 171s</p>	<p>Do you see evidence of thermal injury during the bed dissection, and if so, how would you characterize it?</p>  <p>0s 182s 345s</p>	<p>Do you think acute inflammation of the gallbladder is present at this stage? What features lead you to that conclusion?</p>  <p>82s 575s 657s</p>
<p>Answer: No. the two-structure criterion is not achieved. Only one structure is distinctly visible as tubular, while the other is obscured or insufficiently dissected. The incomplete dissection and possible occlusion by surrounding tissue prevent the clear identification of two tubular structures connected to the gallbladder.</p>	<p>Answer: About 4/10. Both proximal and distal clips are applied, but the spacing and clip-to-cut margin look a bit tight and the clip angles aren't perfectly perpendicular to the duct. Hemostasis is fine, but the construct is short and not as secure or elegant as ideal.</p>	<p>Answer: Yes—there's a minor, superficial thermal contact on less vital tissue, suggested by a faint blanching/singe without structural damage. It's an isolated event without impact on critical structures.</p>	<p>Answer: Yes. The early survey shows a reactive, thickened-appearing gallbladder with surrounding tissue changes consistent with acute inflammation. The tissue looks angry and taut rather than supple, which pushes this toward a moderate-difficulty profile on the Nassar scale.</p>
<p>LLaVA-Video: The video does not provide enough information to determine if the two-structure criterion is achieved. The two-structure criterion is a concept in medical imaging that refers to the ability to distinguish between two different structures or tissues within an image. However, the video only shows a close-up view of a biological tissue with various colors and textures, but it does not provide any clear evidence of two distinct structures or tissues that can be distinguished from each other. Therefore, it is not possible to conclude whether the two-structure criterion is achieved based on the information provided in the video. {Correctness: 25, 'Relevance': 35, 'Linguistic': 60}</p>	<p>LLaVA-Video: The description does not provide enough information to accurately rate the cystic duct clipping and division on a 2-10 performance scale. A rating would require an assessment of the technique, precision, and outcome of the procedure, which cannot be determined from the given information. {Correctness: 0, 'Relevance': 0, 'Linguistic': 0}</p>	<p>LLaVA-Video: The video shows a surgical procedure being performed on the internal anatomy of a patient. The view is through an endoscope, which allows for a close-up look at the surgical site. The area appears to be part of the gastrointestinal tract, possibly the colon or rectum, given the visible layers of tissue and the presence of what looks like a segment of bowel. {Correctness: 10, 'Relevance': 20, 'Linguistic': 20}</p>	<p>LLaVA-Video: The gallbladder is a small, pear-shaped organ located beneath the liver. It stores bile produced by the liver and gallbladder, which is then released into the small intestine to aid in digestion. Inflammation of the gallbladder, known as cholecystitis, can occur due to various reasons such as gallstones, infection, or inflammation of the gallbladder wall. The symptoms of acute cholecystitis include severe abdominal pain, often on the right side, nausea, vomiting, and fever. The presence of these symptoms can indicate that acute inflammation of the gallbladder is present at this stage. {Correctness: 10, 'Relevance': 15, 'Linguistic': 20}</p>
<p>LLaVA-Video-ft: Yes, the two-structure criterion is achieved. The cystic duct and cystic artery are both clearly visible as tubular structures connected to the gallbladder. There are no additional tubular structures present, and the dissection appears sufficient to confirm this criterion. {Correctness: 0, 'Relevance': 60, 'Linguistic': 90}</p>	<p>LLaVA-Video-ft: I'd score it a 2. The clips placement appears suboptimal with limited cuff length and some misalignment, suggesting the duct isn't perfectly aligned or the clip spacing is tight. It's better than a completely inaccurate application, but not as secure or well-spaced as ideal. {Correctness: 35, 'Relevance': 70, 'Linguistic': 80}</p>	<p>LLaVA-Video-ft: I don't see thermal injury. Energy use appears controlled, there's no charring, blanching, or tissue contraction on adjacent vital structures, and the liver bed remains glossy without whitening or delayed oozing. {Correctness: 0, 'Relevance': 50, 'Linguistic': 70}</p>	<p>LLaVA-Video-ft: I don't see thermal injury. Energy use appears controlled, there's no charring, blanching, or tissue contraction on adjacent vital structures, and the liver bed remains glossy without whitening or delayed oozing. {Correctness: 0, 'Relevance': 0, 'Linguistic': 80}</p>
<p>Ours: The cystic duct and cystic artery are not clearly visible as two distinct tubular structures connected to the gallbladder. The view is obstructed by undissected tissue, and the dissection appears incomplete. This prevents confirmation of the two-structure criterion. {Correctness: 90, 'Relevance': 95, 'Linguistic': 90}</p>	<p>Ours: The cystic duct clipping and division appear to be performed with a moderate level of technical skill. The clips placement is secure, but the dissection and clip application are precise, but there is no evidence of excessive bleeding or bile leakage. {Correctness: 60, 'Relevance': 70, 'Linguistic': 60}</p>	<p>Ours: The tissue shows blanching and chging, with a charred spot on the liver bed. I'd classify this as superficial thermal injury to less vital tissue. {Correctness: 85, 'Relevance': 90, 'Linguistic': 80}</p>	<p>Ours: The gallbladder appears tense and distended, with a thickened wall and a bluish-green hue. The peritoneum over the gallbladder looks inflamed and edematous, and there's a reactive sheen of hyperemia on the surface. These features are consistent with acute inflammation, which would raise difficulty on the Parkland Grading Scale and suggest early, careful dissection to avoid perforation or bile spillage. {Correctness: 90, 'Relevance': 85, 'Linguistic': 80}</p>

Fig. 10: Qualitative comparison of model responses on assessment-level tasks with key answer highlighted with red color font. The figure demonstrates how our SurgTEMP generates clinically accurate and contextually appropriate responses for tasks including CVS, difficulty findings, IAE, and skill proficiency assessment, compared to baseline models.

- Pang, B., Montgomery, C., Pietrzyk, P., Ritter, M., Piergiovanni, A., Minderer, M., Pavetic, F., Waters, A., Li, G., Alabdulmohsin, I., Beyler, L., Amelot, J., Lee, K., Steiner, A.P., Li, Y., Keyser, D., Arnab, A., Xu, Y., Rong, K., Kolesnikov, A., Seyedhosseini, M., Angelova, A., Zhai, X., Hously, N., Soricut, R., 2023a. Pali-x: On scaling up a multilingual vision and language model. URL: <https://arxiv.org/abs/2305.18565>, arXiv:2305.18565.
- Chen, X., Wang, X., Changpin, S., Piergiovanni, A., Padlewski, P., Salz, D., Goodman, S., Grycner, A., Mustafa, B., Beyler, L., Kolesnikov, A., Puigcerver, J., Ding, N., Rong, K., Akbari, H., Mishra, G., Xue, L., Thapliyal, A., Bradbury, J., Kuo, W., Seyedhosseini, M., Jia, C., Ayan, B.K., Riquelme, C., Steiner, A., Angelova, A., Zhai, X., Hously, N., Soricut, R., 2023b. Pali: A jointly-scaled multilingual language-image model. URL: <https://arxiv.org/abs/2209.06794>, arXiv:2209.06794.
- da Costa Rocha, C., Padoy, N., Rosa, B., 2019. Self-supervised surgical tool segmentation using kinematic information. URL: <https://arxiv.org/abs/1902.04810>, arXiv:1902.04810.
- DeepSeek-AI, 2024. Deepseek-v3 technical report. URL: <https://arxiv.org/abs/2412.19437>, arXiv:2412.19437.
- DeepSeek-AI, Liu, A., Feng, B., Xue, B., Wang, B., Wu, B., Lu, C., Zhao, C., Deng, C., Zhang, C., Ruan, C., Dai, D., Guo, D., Yang, D., Chen, D., Ji, D., Li, E., Lin, F., Dai, F., Luo, F., Hao, G., Chen, G., Li, G., Zhang, H., Bao, H., Xu, H., Wang, H., Zhang, H., Ding, H., Xin, H., Gao, H., Li, H., Qu, H., Cai, J.L., Liang, J., Guo, J., Ni, J., Li, J., Wang, J., Chen, J., Chen, J., Yuan, J., Qiu, J., Li, J., Song, J., Dong, K., Hu, K., Gao, K., Guan, K., Huang, K., Yu, K., Wang, L., Zhang, L., Xu, L., Xia, L., Zhao, L., Wang, L., Zhang, L., Li, M., Wang, M., Zhang, M., Zhang, M., Tang, M., Li, M., Tian, N., Huang, P., Wang, P., Zhang, P., Wang, Q., Zhu, Q., Chen, Q., Du, Q., Chen, R.J., Jin, R.L., Ge, R., Zhang, R., Pan, R., Wang, R., Xu, R., Zhang, R., Chen, R., Li, S.S., Lu, S., Zhou, S., Chen, S., Wu, S., Ye, S., Ye, S., Ma, S., Wang, S., Zhou, S., Yu, S., Zhou, S., Pan, S., Wang, T., Yun, T., Pei, T., Sun, T., Xiao, W.L., Zeng, W., Zhao, W., An, W., Liu, W., Liang, W., Gao, W., Yu, W., Zhang, W., Li, X.Q., Jin, X., Wang, X., Bi, X., Liu, X., Wang, X., Shen, X., Chen, X., Zhang, X., Chen, X., Nie, X., Sun, X., Wang, X., Cheng, X., Liu, X., Xie, X., Liu, X., Yu, X., Song, X., Shan, X., Zhou, X., Yang, X., Li, X., Su, X., Lin, X., Li, Y.K., Wang, Y.Q., Wei, Y.X., Zhu, Y.X., Zhang, Y., Xu, Y., Xu, Y., Huang, Y., Li, Y., Zhao, Y., Sun, Y., Li, Y., Wang, Y., Yu, Y., Zheng, Y., Zhang, Y., Shi, Y., Xiong, Y., He, Y., Tang, Y., Piao, Y., Wang, Y., Tan, Y., Ma, Y., Liu, Y., Guo, Y., Wu, Y., Ou, Y., Zhu, Y., Wang, Y., Gong, Y., Zou, Y., He, Y., Zha, Y., Xiong, Y., Ma, Y., Yan, Y., Luo, Y., You, Y., Liu, Y., Zhou, Y., Wu, Z.F., Ren, Z.Z., Ren, Z., Sha, Z., Fu, Z., Xu, Z., Huang, Z., Zhang, Z., Xie, Z., Zhang, Z., Hao, Z., Gou, Z., Ma, Z., Yan, Z., Shao, Z., Xu, Z., Wu, Z., Zhang, Z., Li, Z., Gu, Z., Zhu, Z., Liu, Z., Li, Z., Xie, Z., Song, Z., Gao, Z., Pan, Z., 2025. Deepseek-v3 technical report. URL: <https://arxiv.org/abs/2412.19437>, arXiv:2412.19437.
- Gao, Y., Vedula, S.S., Reiley, C.E., Ahmadi, N., Varadarajan, B., Lin, H.C., Tao, L., Zappella, L., Béjar, B., Yuh, D.D., et al., 2014. Jhu-isi gesture and skill assessment working set (jigsaws): A surgical activity dataset for human motion modeling, in: MICCAI workshop: M2cai, p. 3.
- Gurari, D., Li, Q., Stangl, A.J., Guo, A., Lin, C., Grauman, K., Luo, J., Bigham, J.P., 2018. Vizwiz grand challenge: Answering visual questions from blind people. URL: <https://arxiv.org/abs/1802.08218>, arXiv:1802.08218.
- Hasan, M.K., Calvet, L., Rabbani, N., Bartoli, A., 2021. Detection, segmentation, and 3d pose estimation of surgical tools using convolutional neural networks and algebraic geometry. Medical Image Analysis 70, 101994.
- He, R., Xu, M., Das, A., Khan, D.Z., Bano, S., Marcus, H.J., Stoyanov, D., Clarkson, M.J., Islam, M., 2024. Pitvqa: Image-grounded text embedding llm for visual question answering in pituitary surgery, in: International Conference on Medical Image Computing and Computer-Assisted Intervention, Springer. pp. 488–498.
- Hu, M., Xia, P., Wang, L., Yan, S., Tang, F., Xu, Z., Luo, Y., Song, K., Leitner, J., Cheng, X., et al., 2024. Ophnet: A large-scale video benchmark for ophthalmic surgical workflow understanding, in: European Conference on Computer Vision, Springer. pp. 481–500.
- Huang, S., Dong, L., Wang, W., Hao, Y., Singhal, S., Ma, S., Lv, T., Cui, L., Mohammed, O.K., Patra, B., Liu, Q., Aggarwal, K., Chi, Z., Björck, J., Chaudhary, V., Som, S., Song, X., Wei, F., 2023. Language is not all you need: Aligning perception with language models. URL: <https://arxiv.org/abs/2302.14045>, arXiv:2302.14045.
- Hudson, D.A., Manning, C.D., 2019. Gqa: A new dataset for real-world visual reasoning and compositional question answering. URL: <https://arxiv.org/abs/1902.09506>, arXiv:1902.09506.
- Jaspers, T.J., de Jong, R.L., Li, Y., Kusters, C.H., Bakker, F.H., van Jaarsveld, R.C., Kuiper, G.M., van Hillegerberg, R., Ruurda, J.P., Brinkman, W.M., et al., 2025. Scaling up self-supervised learning for improved surgical found-



Fig. 11: Qualitative comparison of model responses on reasoning-level tasks. The figure illustrates how our SurgTEMP generates comprehensive detailed descriptions and performs complex hypothetical reasoning about surgical scenarios, demonstrating superior temporal understanding and clinical reasoning capabilities compared to baseline models.

dation models. arXiv preprint arXiv:2501.09436 .
 Jiang, A.Q., Sablayrolles, A., Roux, A., Mensch, A., Savary, B., Bamford, C., Chaplot, D.S., de las Casas, D., Hanna, E.B., Bressand, F., Lengyel, G., Bour, G., Lample, G., Lavaud, L.R., Saulnier, L., Lachaux, M.A., Stock, P., Subramanian, S., Yang, S., Antoniak, S., Scao, T.L., Gervet, T., Lavril, T., Wang, T., Lacroix, T., Sayed, W.E., 2024. Mixtral of experts. URL:

<https://arxiv.org/abs/2401.04088>, arXiv:2401.04088.
 Laurençon, H., Tronchon, L., Cord, M., Sanh, V., 2024. What matters when building vision-language models? URL: <https://arxiv.org/abs/2405.02246>, arXiv:2405.02246.
 Li, B., Wang, R., Wang, G., Ge, Y., Ge, Y., Shan, Y., 2023a. Seed-bench: Benchmarking multimodal llms with generative comprehension. URL:

- <https://arxiv.org/abs/2307.16125>, arXiv:2307.16125.
- Li, B., Zhang, Y., Chen, L., Wang, J., Pu, F., Cahyono, J.A., Yang, J., Liu, Z., 2025. Otter: A multi-modal model with in-context instruction tuning. URL: <https://arxiv.org/abs/2305.03726>, arXiv:2305.03726.
- Li, C., Xu, H., Tian, J., Wang, W., Yan, M., Bi, B., Ye, J., Chen, H., Xu, G., Cao, Z., Zhang, J., Huang, S., Huang, F., Zhou, J., Si, L., 2022. mplug: Effective and efficient vision-language learning by cross-modal skip-connections. URL: <https://arxiv.org/abs/2205.12005>, arXiv:2205.12005.
- Li, F., Zhang, R., Zhang, H., Zhang, Y., Li, B., Li, W., Ma, Z., Li, C., 2024a. Llava-next-interleave: Tackling multi-image, video, and 3d in large multimodal models. URL: <https://arxiv.org/abs/2407.07895>, arXiv:2407.07895.
- Li, J., Li, D., Savarese, S., Hoi, S., 2023b. Blip-2: Bootstrapping language-image pre-training with frozen image encoders and large language models. URL: <https://arxiv.org/abs/2301.12597>, arXiv:2301.12597.
- Li, K., He, Y., Wang, Y., Li, Y., Wang, W., Luo, P., Wang, Y., Wang, L., Qiao, Y., 2024b. Videochat: Chat-centric video understanding. URL: <https://arxiv.org/abs/2305.06355>, arXiv:2305.06355.
- Lin, B., Ye, Y., Zhu, B., Cui, J., Ning, M., Jin, P., Yuan, L., 2024a. Video-llava: Learning united visual representation by alignment before projection. URL: <https://arxiv.org/abs/2311.10122>, arXiv:2311.10122.
- Lin, J., Yin, H., Ping, W., Lu, Y., Molchanov, P., Tao, A., Mao, H., Kautz, J., Shooeybi, M., Han, S., 2024b. Vila: On pre-training for visual language models. URL: <https://arxiv.org/abs/2312.07533>, arXiv:2312.07533.
- Liu, D., Li, Q., Jiang, T., Wang, Y., Miao, R., Shan, F., Li, Z., 2021. Towards unified surgical skill assessment, in: Proceedings of the IEEE/CVF conference on computer vision and pattern recognition, pp. 9522–9531.
- Liu, H., Li, C., Wu, Q., Lee, Y.J., 2023. Visual instruction tuning. URL: <https://arxiv.org/abs/2304.08485>, arXiv:2304.08485.
- Liu, Y., Duan, H., Zhang, Y., Li, B., Zhang, S., Zhao, W., Yuan, Y., Wang, J., He, C., Liu, Z., Chen, K., Lin, D., 2024. Mmbench: Is your multi-modal model an all-around player? URL: <https://arxiv.org/abs/2307.06281>, arXiv:2307.06281.
- Luengo, I., Grammatikopoulou, M., Mohammadi, R., Walsh, C., Nwoye, C.I., Alapatt, D., Padoy, N., Ni, Z.L., Fan, C.C., Bian, G.B., Hou, Z.G., Ha, H., Wang, J., Wang, H., Guo, D., Wang, L., Wang, G., Islam, M., Giddwani, B., Hongliang, R., Pissas, T., Ravasio, C., Huber, M., Birch, J., Rio, J.M.N.D., da Cruz, L., Bergeles, C., Chen, H., Jia, F., KumarTomar, N., Jha, D., Riegler, M.A., Halvorsen, P., Bano, S., Vaghela, U., Hong, J., Ye, H., Huang, F., Wang, D.H., Stoyanov, D., 2022. 2020 cataracts semantic segmentation challenge. URL: <https://arxiv.org/abs/2110.10965>, arXiv:2110.10965.
- Maaz, M., Rasheed, H., Khan, S., Khan, F., 2024a. Videogpt+: Integrating image and video encoders for enhanced video understanding. URL: <https://arxiv.org/abs/2406.09418>, arXiv:2406.09418.
- Maaz, M., Rasheed, H., Khan, S., Khan, F.S., 2024b. Video-chatgpt: Towards detailed video understanding via large vision and language models. URL: <https://arxiv.org/abs/2306.05424>, arXiv:2306.05424.
- Marino, K., Rastegari, M., Farhadi, A., Mottaghi, R., 2019. Ok-vqa: A visual question answering benchmark requiring external knowledge. URL: <https://arxiv.org/abs/1906.00067>, arXiv:1906.00067.
- Martin, J., Regehr, G., Reznick, R., Macrae, H., Murnaghan, J., Hutchison, C., Brown, M., 1997. Objective structured assessment of technical skill (osats) for surgical residents. *British journal of surgery* 84, 273–278.
- Mascagni, P., Alapatt, D., Garcia, A., Okamoto, N., Vardazaryan, A., Costamagna, G., Dallemagne, B., Padoy, N., 2021a. Surgical data science for safe cholecystectomy: a protocol for segmentation of hepatocystic anatomy and assessment of the critical view of safety. URL: <https://arxiv.org/abs/2106.10916>, arXiv:2106.10916.
- Mascagni, P., Alapatt, D., Murali, A., Vardazaryan, A., Garcia, A., Okamoto, N., Costamagna, G., Mutter, D., Marescaux, J., Dallemagne, B., Padoy, N., 2025. Endoscapes, a critical view of safety and surgical scene segmentation dataset for laparoscopic cholecystectomy. *Scientific Data* 12, 331. URL: <https://doi.org/10.1038/s41597-025-04642-4>, doi:10.1038/s41597-025-04642-4.
- Mascagni, P., Fiorillo, C., Urade, T., Emre, T., Yu, T., Wakabayashi, T., Felli, E., Perretta, S., Swannstrom, L., Mutter, D., et al., 2020. Formalizing video documentation of the critical view of safety in laparoscopic cholecystectomy: a step towards artificial intelligence assistance to improve surgical safety. *Surgical endoscopy* 34, 2709–2714.
- Mascagni, P., Rodríguez-Luna, M.R., Urade, T., Felli, E., Pessaux, P., Mutter, D., Marescaux, J., Costamagna, G., Dallemagne, B., Padoy, N., 2021b. Intraoperative time-out to promote the implementation of the critical view of safety in laparoscopic cholecystectomy: A video-based assessment of 343 procedures. *Journal of the American College of Surgeons* 233, 497–505. URL: <http://dx.doi.org/10.1016/j.jamcollsurg.2021.06.018>, doi:10.1016/j.jamcollsurg.2021.06.018.
- Meyer, A., Arboit, L., Massimiani, G., Brucchi, F., Amodio, L.E., Mutter, D., Padoy, N., 2025. S4m: Segment anything with 4 extreme points. URL: <https://arxiv.org/abs/2503.05534>, arXiv:2503.05534.
- Meyer, A., Mazellier, J.P., Dana, J., Padoy, N., 2024. On-the-fly point annotation for fast medical video labeling. *International Journal of Computer Assisted Radiology and Surgery* 19, 1093–1101. URL: <http://dx.doi.org/10.1007/s11548-024-03098-y>, doi:10.1007/s11548-024-03098-y.
- Murali, A., Alapatt, D., Mascagni, P., Vardazaryan, A., Garcia, A., Okamoto, N., Mutter, D., Padoy, N., 2023a. Encoding surgical videos as latent spatiotemporal graphs for object and anatomy-driven reasoning, in: International Conference on Medical Image Computing and Computer-Assisted Intervention, Springer, pp. 647–657.
- Murali, A., Alapatt, D., Mascagni, P., Vardazaryan, A., Garcia, A., Okamoto, N., Mutter, D., Padoy, N., 2023b. Latent graph representations for critical view of safety assessment. *IEEE Transactions on Medical Imaging* , 1–1doi:10.1109/TMI.2023.3333034.
- Murali, A., Zarin, F., Meyer, A., Mascagni, P., Mutter, D., Padoy, N., 2025. Cyclesam: Few-shot surgical scene segmentation with cycle- and scene-consistent feature matching. URL: <https://arxiv.org/abs/2407.06795>, arXiv:2407.06795.
- Nwoye, C.I., Gonzalez, C., Yu, T., Mascagni, P., Mutter, D., Marescaux, J., Padoy, N., 2020. Recognition of Instrument-Tissue Interactions in Endoscopic Videos via Action Triplets. Springer International Publishing. p. 364–374. URL: http://dx.doi.org/10.1007/978-3-030-59716-0_35, doi:10.1007/978-3-030-59716-0_35.
- Nwoye, C.I., Mutter, D., Marescaux, J., Padoy, N., 2019. Weakly supervised convolutional lstm approach for tool tracking in laparoscopic videos. *International Journal of Computer Assisted Radiology and Surgery* 14, 1059–1067. URL: <http://dx.doi.org/10.1007/s11548-019-01958-6>, doi:10.1007/s11548-019-01958-6.
- Nwoye, C.I., Yu, T., Gonzalez, C., Seeliger, B., Mascagni, P., Mutter, D., Marescaux, J., Padoy, N., 2022. Rendezvous: Attention mechanisms for the recognition of surgical action triplets in endoscopic videos. *Medical Image Analysis* 78, 102433. URL: <http://dx.doi.org/10.1016/j.media.2022.102433>, doi:10.1016/j.media.2022.102433.
- Nwoye, C.I., Yu, T., Sharma, S., Murali, A., Alapatt, D., Vardazaryan, A., Yuan, K., Hajek, J., Reiter, W., Yamlihi, A., Smidt, F.H., Zou, X., Zheng, G., Oliveira, B., Torres, H.R., Kondo, S., Kasai, S., Holm, F., Özsoy, E., Gui, S., Li, H., Raviteja, S., Sathish, R., Poudel, P., Bhattarai, B., Wang, Z., Rui, G., Schellenberg, M., Vilaça, J.L., Czempiel, T., Wang, Z., Sheet, D., Thapa, S.K., Berniker, M., Godau, P., Morais, P., Regmi, S., Tran, T.N., Fonseca, J., Nölke, J.H., Lima, E., Vazquez, E., Maier-Hein, L., Navab, N., Mascagni, P., Seeliger, B., Gonzalez, C., Mutter, D., Padoy, N., 2023. Cholectriplet2022: Show me a tool and tell me the triplet — an endoscopic vision challenge for surgical action triplet detection. *Medical Image Analysis* 89, 102888. URL: <http://dx.doi.org/10.1016/j.media.2023.102888>, doi:10.1016/j.media.2023.102888.
- OpenAI, :, Agarwal, S., Ahmad, L., Ai, J., Altman, S., Applebaum, A., Arbus, E., Arora, R.K., Bai, Y., Baker, B., Bao, H., Barak, B., Bennett, A., Bertao, T., Brett, N., Brevdo, E., Brockman, G., Bubeck, S., Chang, C., Chen, K., Chen, M., Cheung, E., Clark, A., Cook, D., Dukhan, M., Dvorak, C., Fives, K., Fomenko, V., Garipov, T., Georgiev, K., Glaese, M., Gogineni, T., Goucher, A., Gross, L., Guzman, K.G., Hallman, J., Hehir, J., Heidecke, J., Helyar, A., Hu, H., Huet, R., Huh, J., Jain, S., Johnson, Z., Koch, C., Kofman, I., Kundel, D., Kwon, J., Kyrylov, V., Le, E.Y., Leclerc, G., Lennon, J.P., Lessans, S., Lezcano-Casado, M., Li, Y., Li, Z., Lin, J., Liss, J., Lily, Liu, Liu, J., Lu, K., Lu, C., Martinovic, Z., McCallum, L., McGrath, J., McKinney, S., McLaughlin, A., Mei, S., Mostovoy, S., Mu, T., Myles, G., Neitz, A., Nichol, A., Pachocki, J., Paino, A., Palmie, D., Pantuliano, A., Parascandolo, G., Park, J., Pathak, L., Paz, C., Peran, L., Pimenov, D., Pokrass, M., Proehl, E., Qiu, H., Raila, G., Raso, F., Ren, H., Richardson, K., Robinson, D., Rotsted, B., Salman, H., Sanjeev, S., Schwarzer, M., Sculley, D., Sikchi, H., Simon, K., Singhal, K., Song, Y., Stuckey, D., Sun, Z., Tillet, P., Toizer, S., Tsimpouras, F., Vyas, N., Wallace, E., Wang, X., Wang, M., Watkins, O., Weil, K., Wendling, A., Whinnery, K., Whitney, C., Wong, H., Yang, L., Yang, Y., Yasunaga, M., Ying, K., Zaremba, W., Zhan, W., Zhang, C., Zhang, B., Zhang, E., Zhao, S., 2025. gpt-oss-120b and gpt-oss-20b model card. URL: <https://arxiv.org/abs/2508.10925>, arXiv:2508.10925.
- OpenAI, Achiam, J., Adler, S., Agarwal, S., Ahmad, L., Akkaya, I., Aleman, F.L., Almeida, D., Altenschmidt, J., Altman, S., Anadkat, S., Avila, R., Babuschkin, I., Balaji, S., Balcom, V., Baltescu, P., Bao, H., Bavarian, M., Belgum, J., Bello, I., Berdine, J., Bernadett-Shapiro, G., Berner, C., Bogdonoff, L., Boiko, O., Boyd, M., Brakman, A.L., Brockman, G., Brooks, T., Brundage, M., Button, K., Cai, T., Campbell, R., Cann, A., Carey, B., Carlson, C., Carmichael, R., Chan, B., Chang, C., Chantzis, F., Chen, D., Chen, S., Chen, R., Chen, J., Chen, M., Chess, B., Cho, C., Chu,

- C., Chung, H.W., Cummings, D., Currier, J., Dai, Y., Decareaux, C., Degry, T., Deutsch, N., Deville, D., Dhar, A., Dohan, D., Dowling, S., Dunning, S., Ecoffet, A., Eleti, A., Eloundou, T., Farhi, D., Fedus, L., Felix, N., Fishman, S.P., Forte, J., Fulford, I., Gao, L., Georges, E., Gibson, C., Goel, V., Gogineni, T., Goh, G., Gontijo-Lopes, R., Gordon, J., Grafstein, M., Gray, S., Greene, R., Gross, J., Gu, S.S., Guo, Y., Hallacy, C., Han, J., Harris, J., He, Y., Heaton, M., Heidecke, J., Hesse, C., Hickey, A., Hickey, W., Hoeschele, P., Houghton, B., Hsu, K., Hu, S., Hu, X., Huizinga, J., Jain, S., Jain, S., Jang, J., Jiang, A., Jiang, R., Jin, H., Jin, D., Jomoto, S., Jonn, B., Jun, H., Kaftan, T., Łukasz Kaiser, Kamali, A., Kanitscheider, I., Keskar, N.S., Khan, T., Kilpatrick, L., Kim, J.W., Kim, C., Kim, Y., Kirchner, J.H., Kiros, J., Knight, M., Kokotajlo, D., Łukasz Kondraciuk, Kondrich, A., Konstantinidis, A., Kosic, K., Krueger, G., Kuo, V., Lampe, M., Lan, I., Lee, T., Leike, J., Leung, J., Levy, D., Li, C.M., Lim, R., Lin, M., Lin, S., Litwin, M., Lopez, T., Lowe, R., Lue, P., Makanju, A., Malfacini, K., Manning, S., Markov, T., Markovski, Y., Martin, B., Mayer, K., Mayne, A., McGrew, B., McKinney, S.M., McLeavey, C., McMillan, P., McNeil, J., Medina, D., Mehta, A., Menick, J., Metz, L., Mishchenko, A., Mishkin, P., Monaco, V., Morikawa, E., Mossing, D., Mu, T., Murati, M., Murk, O., Mély, D., Nair, A., Nakano, R., Nayak, R., Neelakantan, A., Ngo, R., Noh, H., Ouyang, L., O'Keefe, C., Pachocki, J., Paino, A., Palermo, J., Pantuliano, A., Parascandolo, G., Parish, J., Parparita, E., Passos, A., Pavlov, M., Peng, A., Perelman, A., de Avila Belbute Peres, F., Petrov, M., de Oliveira Pinto, H.P., Michael, Pokorný, Pokrass, M., Pong, V.H., Powell, T., Power, A., Power, B., Proehl, E., Puri, R., Radford, A., Rae, J., Ramesh, A., Raymond, C., Real, F., Rimbach, K., Ross, C., Rotsted, B., Roussez, H., Ryder, N., Saltarelli, M., Sanders, T., Santurkar, S., Sastry, G., Schmidt, H., Schnurr, D., Schulman, J., Selsam, D., Sheppard, K., Sherbakov, T., Shieh, J., Shoker, S., Shyam, P., Sidor, S., Sigler, E., Simens, M., Sitkin, J., Slama, K., Sohl, I., Sokolowsky, B., Song, Y., Staudacher, N., Such, F.P., Summers, N., Sutskever, I., Tang, J., Tezak, N., Thompson, M.B., Tillet, P., Tootoonchian, A., Tseng, E., Tuggle, P., Turley, N., Tworek, J., Uribe, J.F.C., Vallone, A., Vijayvergiya, A., Voss, C., Wainwright, C., Wang, J.J., Wang, A., Wang, B., Ward, J., Wei, J., Weinmann, C., Welihinda, A., Welinder, P., Weng, J., Weng, L., Wiethoff, M., Willner, D., Winter, C., Wolrich, S., Wong, H., Workman, L., Wu, S., Wu, J., Wu, M., Xiao, K., Xu, T., Yoo, S., Yu, K., Yuan, Q., Zaremba, W., Zellers, R., Zhang, C., Zhang, M., Zhao, S., Zheng, T., Zhuang, J., Zhuk, W., Zoph, B., 2024. Gpt-4 technical report. URL: <https://arxiv.org/abs/2303.08774>, arXiv:2303.08774.
- Pedrett, R., Mascagni, P., Beldi, G., Padoy, N., Lavanchy, J.L., 2023. Technical skill assessment in minimally invasive surgery using artificial intelligence: a systematic review. *Surgical endoscopy* 37, 7412–7424.
- Pei, J., Zhang, J., Qin, G., Wang, K., Jin, Y., Heng, P.A., 2025. Instrument-tissue-guided surgical action triplet detection via textual-temporal trail exploration. *IEEE Transactions on Medical Imaging* 44, 5278–5289. doi:10.1109/TMI.2025.3590457.
- Peng, Z., Wang, W., Dong, L., Hao, Y., Huang, S., Ma, S., Wei, F., 2023. Kosmos-2: Grounding multimodal large language models to the world. URL: <https://arxiv.org/abs/2306.14824>, arXiv:2306.14824.
- Schwenk, D., Khandelwal, A., Clark, C., Marino, K., Mottaghi, R., 2022. Aokvqa: A benchmark for visual question answering using world knowledge. URL: <https://arxiv.org/abs/2206.01718>, arXiv:2206.01718.
- Seenivasan, L., Islam, M., Krishna, A.K., Ren, H., 2022. Surgical-vqa: Visual question answering in surgical scenes using transformer, in: International Conference on Medical Image Computing and Computer-Assisted Intervention, Springer. pp. 33–43.
- Sharma, S., Nwoye, C.I., Mutter, D., Padoy, N., 2023a. Rendezvous in time: an attention-based temporal fusion approach for surgical triplet recognition. *International Journal of Computer Assisted Radiology and Surgery* 18, 1053–1059. URL: <http://dx.doi.org/10.1007/s11548-023-02914-1>, doi:10.1007/s11548-023-02914-1.
- Sharma, S., Nwoye, C.I., Mutter, D., Padoy, N., 2023b. Surgical action triplet detection by mixed supervised learning of instrument-tissue interactions. URL: <https://arxiv.org/abs/2307.09548>, arXiv:2307.09548.
- Sharma, S., Vannucci, M., Pestana Legori, L., Scaglia, M., Laracca, G.G., Mutter, D., Alfieri, S., Mascagni, P., Padoy, N., 2025. Early operative difficulty assessment in laparoscopic cholecystectomy via snapshot-centric video analysis. *International Journal of Computer Assisted Radiology and Surgery* 20, 1185–1193. URL: <http://dx.doi.org/10.1007/s11548-025-03372-7>, doi:10.1007/s11548-025-03372-7.
- Tao, R., Zou, X., Zheng, G., 2023. Last: Latent space-constrained transformers for automatic surgical phase recognition and tool presence detection. *IEEE Transactions on Medical Imaging* 42, 3256–3268.
- Vannucci, M., Laracca, G.G., Mercantini, P., Perretta, S., Padoy, N., Dalle-magne, B., Mascagni, P., 2022. Statistical models to preoperatively predict operative difficulty in laparoscopic cholecystectomy: A systematic review. *Surgery* 171, 1158–1167. URL: <https://www.sciencedirect.com/science/article/pii/S0039606021009594>, doi:<https://doi.org/10.1016/j.surg.2021.10.001>.
- Vlontzos, A., Alansary, A., Kamnitsas, K., Rueckert, D., Kainz, B., 2019. Multiple landmark detection using multi-agent reinforcement learning. URL: <https://arxiv.org/abs/1907.00318>, arXiv:1907.00318.
- Wagner, M., Müller-Stich, B.P., Kisilenko, A., Tran, D., Heger, P., Mündermann, L., Lubotsky, D.M., Müller, B., Davitashvili, T., Capek, M., et al., 2023. Comparative validation of machine learning algorithms for surgical workflow and skill analysis with the heichole benchmark. *Medical Image Analysis* 86, 102770.
- Wagner, M., Müller-Stich, B.P., Kisilenko, A., Tran, D., Heger, P., Mündermann, L., Lubotsky, D.M., Müller, B., Davitashvili, T., Capek, M., Reinke, A., Yu, T., Vardazaryan, A., Nwoye, C.I., Padoy, N., Liu, X., Lee, E.J., Disch, C., Meine, H., Xia, T., Jia, F., Kondo, S., Reiter, W., Jin, Y., Long, Y., Jiang, M., Dou, Q., Heng, P.A., Twick, I., Kirtac, K., Hosgor, E., Bolmgren, J.L., Stenzel, M., von Siemens, B., Kennigott, H.G., Nickel, F., von Frankenberg, M., Mathis-Ullrich, F., Maier-Hein, L., Speidel, S., Bodenstedt, S., 2021. Comparative validation of machine learning algorithms for surgical workflow and skill analysis with the heichole benchmark. URL: <https://arxiv.org/abs/2109.14956>, arXiv:2109.14956.
- Wang, G., Bai, L., Wang, J., Yuan, K., Li, Z., Jiang, T., He, X., Wu, J., Chen, Z., Lei, Z., Liu, H., Wang, J., Zhang, F., Padoy, N., Navab, N., Ren, H., 2025a. EndoChat: Grounded multimodal large language model for endoscopic surgery. URL: <https://arxiv.org/abs/2501.11347>, arXiv:2501.11347.
- Wang, Y., Li, X., Yan, Z., He, Y., Yu, J., Zeng, X., Wang, C., Ma, C., Huang, H., Gao, J., et al., 2025b. Internvideo2.5: Empowering video mlms with long and rich context modeling. arXiv preprint arXiv:2501.12386.
- Ye, J., Xu, H., Liu, H., Hu, A., Yan, M., Qian, Q., Zhang, J., Huang, F., Zhou, J., 2024. mplug-owl3: Towards long image-sequence understanding in multimodal large language models, in: The Thirteenth International Conference on Learning Representations.
- Yu, W., Yang, Z., Li, L., Wang, J., Lin, K., Liu, Z., Wang, X., Wang, L., 2024. Mm-vet: Evaluating large multimodal models for integrated capabilities. URL: <https://arxiv.org/abs/2308.02490>, arXiv:2308.02490.
- Yuan, K., Kattel, M., Lavanchy, J.L., Navab, N., Srivastav, V., Padoy, N., 2024. Advancing surgical vqa with scene graph knowledge. *International Journal of Computer Assisted Radiology and Surgery* 19, 1409–1417.
- Zhai, X., Mustafa, B., Kolesnikov, A., Beyer, L., 2023. Sigmoid loss for language image pre-training, in: Proceedings of the IEEE/CVF international conference on computer vision, pp. 11975–11986.
- Zhang, P., Zhang, K., Li, B., Zeng, G., Yang, J., Zhang, Y., Wang, Z., Tan, H., Li, C., Liu, Z., 2024a. Long context transfer from language to vision. arXiv preprint arXiv:2406.16852.
- Zhang, Y., Wu, J., Li, W., Li, B., Ma, Z., Liu, Z., Li, C., 2024b. Video instruction tuning with synthetic data. arXiv preprint arXiv:2410.02713.
- Zhang, Y., Wu, J., Li, W., Li, B., Ma, Z., Liu, Z., Li, C., 2025. Llava-video: Video instruction tuning with synthetic data. URL: <https://arxiv.org/abs/2410.02713>, arXiv:2410.02713.
- Zhu, D., Chen, J., Shen, X., Li, X., Elhoseiny, M., 2023. Minigt-4: Enhancing vision-language understanding with advanced large language models. URL: <https://arxiv.org/abs/2304.10592>, arXiv:2304.10592.
- Zia, A., Berniker, M., Nespolo, R.G., Perreault, C., Bhattacharyya, K., Liu, X., Wang, Z., Kondo, S., Kasai, S., Hirasawa, K., Liu, B., Austin, D., Wang, Y., Futrega, M., Puget, J.F., Li, Z., Sato, Y., Fujii, R., Hachiuma, R., Masuda, M., Saito, H., Wang, A., Xu, M., Islam, M., Bai, L., Pang, W., Ren, H., Nwoye, C., Sestini, L., Padoy, N., Nielsen, M., Schüttler, S., Sentker, T., Husseini, H., Baltruschat, I., Schmitz, R., Werner, R., Matsun, A., Farooq, M., Saeed, N., Viera, J.R.R., Yaqub, M., Getty, N., Xia, F., Zhao, Z., Duan, X., Yao, X., Lou, A., Yang, H., Han, J., Noble, J., Wu, J.Y., Alshirbaji, T.A., Jalal, N.A., Arabian, H., Ding, N., Moeller, K., Chen, W., He, Q., Bilal, M., Akinosho, T., Qayyum, A., Caputo, M., Vohra, H., Loizou, M., Ajayi, A., Berrou, I., Niyi-Odumosu, F., Budd, C., Alabi, O., Vercauteren, T., Zhao, R., Acar, A., Han, J., Atoum, J., Qin, Y., Wu, J.Y., Hua, S., Ping, L., Wu, W., Wei, R., Wu, J., Pang, Y., Chen, Z., Jaspers, T., Yamlihi, A., Kalinowski, P., Michael, D., dsch, T.R., Hübner, M., Stoyanov, D., Speidel, S., Maier-Hein, L., Jarc, A., 2025. Intuitive surgical surgtoolloc challenge results: 2022-2023. URL: <https://arxiv.org/abs/2305.07152>, arXiv:2305.07152.

Appendix A. Data Generation Prompts

Appendix A.1. CholecT50-Caption-VQA Generation Prompt

The following prompt was used to generate question-answer pairs from expert-annotated surgical video captions for the

CholecT50-Caption-VQA subset:

System Prompt:

You are an experienced surgeon providing expert insights on laparoscopic cholecystectomy procedures.

Task: Generate Question-Answer pairs from expert-annotated video captions following a structured template covering: (1) anatomical space description with visual features and spatial relationships, (2) action recognition, (3) action motivation, (4) procedural errors or deviations, and (5) presence of smoke and lens fouling.

Input Format:

Caption: {caption}

Output Requirements:

Type 1 - Conversational QA: Create targeted questions isolating specific informational aspects (tools, anatomy, actions) from the caption. Generate multiple linguistically variable question-answer pairs in conversational tone. Question quantity should reflect caption content richness rather than template structure.

Type 2 - Descriptive QA: Synthesize multiple caption aspects into comprehensive questions requiring detailed elaboration of the surgical scene. Answers should integrate information holistically across caption elements.

Type 3 - Reasoning QA: Design questions requiring clinical reasoning and surgical expertise beyond explicit visual information. Base reasoning scenarios on action motivation from the caption to assess surgical decision-making and procedural rationale.

Format:

Type 1: Conversational QA

Q1: [question]

A1: [answer]

Q2: [question]

A2: [answer]

...

Type 2: Descriptive QA

Q1: [question]

A1: [answer]

Type 3: Reasoning QA

Q1: [question]

A1: [answer]

Input: Caption: {caption}

Task: Generate Question-Answer pairs from annotated surgical keyframes using CVS annotation guidelines, checklists, and expert examples. Assess whether each CVS criterion is achieved based on visual evidence from color-coded bounding box annotations.

Input Format:

Image: [surgical keyframe]

CVS Label: {CVS_label}

CVS Guidelines: {CVS_instructions}

CVS Annotation Checklist:

{CVS_annotation_checklist}

CVS Annotation Examples: {CVS_flashcards}

Visual Grounding: Detected anatomical structures and tools are annotated with color-coded bounding boxes. Utilize these visual clues in assessment:

- cystic_plate: Green
- calot_triangle: Blue
- cystic_artery: Yellow
- cystic_duct: Magenta
- gallbladder: Cyan
- tool: Red

Output Requirements:

Generate open-ended questions assessing whether each CVS criterion is achieved and why. Questions must not imply answers. Answers should follow step-by-step reasoning processes comparing visual clues with CVS annotation checklist and examples.

Format:

Q1: [question]

A1: [answer]

Q2: [question]

A2: [answer]

Q3: [question]

A3: [answer]

Input: Image: [keyframe], CVS Label: {CVS_label}, CVS Guidelines: {CVS_instructions}, CVS Annotation Checklist: {CVS_annotation_checklist}, CVS Annotation Examples: {CVS_flashcards}

Appendix A.2. Endoscopes-VQA Generation Prompt

The following prompt was used to generate CVS-focused question-answer pairs from annotated surgical keyframes for the Endoscopes-VQA subset:

System Prompt:

You are an experienced surgeon providing expert insights on Critical View of Safety (CVS) achievement in laparoscopic cholecystectomy.

Appendix A.3. CholeScore-VQA Generation Prompt

The following prompt was used to generate phase-level safety assessment question-answer pairs from multi-dimensional annotations for the CholeScore-VQA subset:

System Prompt:

You are an experienced surgeon providing expert insights on laparoscopic cholecystectomy safety assessment.

Task: Generate Question-Answer pairs for a phase-level

surgical video clip using expert annotations from three safety assessment categories: operative difficulty (Nassar, Sugrue, PGS scales), intraoperative adverse events (SE-VERE classification), and technical skill assessment (OS-ATS framework).

Input Format:

Phase:

{surgical_phase}

Findings:

{finding_id} - {finding_name}: {annotation_value}

Description:

{clinical_description}

Output Requirements:

Type 1 - Conversational QA: Create targeted questions isolating individual findings without revealing annotations. Focus on clinical assessment rationale and include finding IDs for traceability.

Type 2 - Descriptive QA: Synthesize all findings into comprehensive safety assessments. Specify relevant scale systems and scores while considering synergistic effects between findings.

Type 3 - Reasoning QA: Design hypothetical scenarios modifying specific findings to assess reasoning about alternative procedural contexts and safety implications.

Format:

Type 1: Conversational QA

{{finding_ID}}

Q1: [question]

A1: [answer]

Type 2: Descriptive QA

Q1: [question]

A1: [answer]

Type 3: Reasoning QA

Q1: [question]

A1: [answer]

Input: Phase: {phase}, Findings: {findings}

Comprehensive Assessment [CA]

Please describe the video clip from the perspective of intra-operative difficulty using established scales.

Answer: In terms of intra-operative difficulty, the scene shows low inflammatory burden. By the Japan-Taiwan-Korea (Iwashita) scale, there is no evidence of 'easy bleeding,' which would otherwise merit a score of 3; here, the bed stays dry with minimal hemostatic activity, so that component does not contribute to difficulty. Likewise, there are no edematous changes (which, when present, score 1 on Iwashita), and I don't see fibrotic tissue bands or dense fibrotic texture (Iwashita categories that score 1-2) nor any scarring (Iwashita partial/diffuse scarring would score 3-4). The absence of these inflammatory and fibrotic markers keeps the dissection plane crisp and predictable. From an anatomic difficulty standpoint using the Nassar grading system, there is no suggestion of a deep, recessed fossa (a finding associated with Grade 3 difficulty); exposure is direct with standard retraction, again indicating lower complexity. Regarding the quality of the bed dissection, on the provided performance rubric for this phase I would assign a score of 5 out of 6: the liver bed remains effectively dry without significant bleeding, there is no bile or stone spillage, and the gallbladder appears nearly entirely intact—better than the 'minimal perforation, dry bed' description for a 4 but shy of a flawless 6. Safety metrics are favorable: there is no bleeding event to grade on the bleeding severity scale, and there are no observable thermal or mechanical injuries, preserving tissue integrity and corroborating controlled energy use and precise instrument handling. Overall, the combined absence of inflammatory difficulty markers (Iwashita), lack of an anatomic deep fossa (Nassar), and a high performance score for the bed dissection indicate a technically efficient, low-difficulty sequence with high-quality execution.

LLaVA-Video: The procedure appears to be a laparoscopic surgery, which is minimally invasive and involves making small incisions in the abdomen. The quality of the operation seems to be high, as the instruments are being used with precision and care. The surgeon is carefully manipulating the tissue and using the appropriate tools to perform the necessary actions. The patient's body is likely being supported by a surgical drape to keep it clean and sterile. The overall atmosphere of the operation is calm and focused, indicating that the surgeon is experienced and skilled in performing this type of surgery.

{'Correctness': 10, 'Relevance': 20, 'Linguistic': 30}

LLaVA-Video-ft: The procedure demonstrates a high level of technical skill and adherence to safety standards.

{'Correctness': 12, 'Relevance': 20, 'Linguistic': 20}

Ours: From a difficulty standpoint, the cystic pedicle dissection appears straightforward. On the Nassar scale, there are no signs of a short or dilated cystic duct (—features that would push the case toward Grade 3—so the pedicle component aligns with a lower grade. There is also no anterior or accessory arterial branch complicating the pedicle, which would otherwise escalate difficulty by adding an extra vascular structure to identify and control. The absence of these features synergizes to reduce the risk profile for this phase: the duct can be identified with standard traction-countertraction, and the pedicle can be cleared without the need for advanced hemostatic maneuvers or bailout strategies. Regarding operative quality, on the provided bleeding severity grading (—where 0 (= none, 2 = very low, 4 = low, 6 = moderate, 8 = high, 10 = very high—there is no bleeding observed, so the grade is effectively 0. This supports a clean field, allowing uninterrupted visualization and precise dissection. On the gallbladder fossa dissection quality scale (—where 1 = perforation with bile/stone spillage, 2 = perforation without spillage, 3 = intact—there is no evidence of gallbladder perforation, so the score is 3. This indicates that the gallbladder remains intact during removal, which is favorable for avoiding postoperative complications such as bile leakage or infection. In combination, the lack of ductal anomalies, absence of arterial variants, and absence of bleeding synergize to keep the pedicle dissection low in difficulty and the overall intra-operative quality high.

{'Correctness': 55, 'Relevance': 70, 'Linguistic': 45}

Intra-operative Planning [IP]

Given limited adhesions confined to the gallbladder body, a mild overall adhesion load, and dense omental adhesions but no hepatic flexure involvement, how would you optimize trocar strategy and initial adhesiolysis to minimize risk and expedite exposure, and would you anticipate needing a bailout?

Answer: I would maintain a standard four-port setup but place the subxiphoid/epigastric port slightly lateral or higher to improve the angle for omental takedown and cephalad traction. The first priority is to free the omentum where it tethers the mid-gallbladder; this restores the ability to elevate the fundus and create tension lines that open safe, avascular planes. With <50% coverage, I would favor blunt-sharp adhesiolysis close to the gallbladder wall, using low-energy, short bursts to protect the transverse colon. Because the fundus is mobile and the hepatic flexure is uninvolved, early fundic retraction will rapidly improve visualization of the infundibulum without resorting to a fundus-first bailout. I would not anticipate a bailout here: once the omental adhesions are cleared, standard exposure of Calot's triangle should be achievable, and the absence of deep lateral or colonic involvement lowers the risk of entry-related or dissection-related complications.

LLaVA-Video: Given the described adhesions, a strategic approach to trocar placement and initial adhesiolysis is crucial to minimize risk and expedite exposure. The initial trocar placement should be chosen to avoid areas of dense adhesions, such as the omentum, to prevent significant bleeding or damage. A 12mm trocar can be used for initial access, allowing for a broad view of the peritoneal cavity and facilitating the identification of any remaining adhesions. Initial adhesiolysis should focus on the areas with mild adhesions, starting from the gallbladder body and working towards the liver. This will help in minimizing the risk of bleeding and damage to surrounding structures. The use of a laparoscopic grasper or dissecting forceps can be employed to gently separate the adhesions without causing significant bleeding. Anticipating a bailout is always prudent, especially when dealing with dense omental adhesions. A backup plan should include having additional trocars ready for further access if needed, as well as being prepared to convert to an open procedure if the adhesions are more extensive than initially anticipated. Regular monitoring of vital signs and hemodynamic stability is essential to ensure patient safety during the procedure.

{'Correctness': 35, 'Relevance': 45, 'Linguistic': 30}

LLaVA-Video-ft: I would plan a standard four-port layout but fine-tune port positioning to optimize angles and minimize risk.

{'Correctness': 18, 'Relevance': 28, 'Linguistic': 24}

Ours: I would plan a standard four-port layout but position the camera port slightly higher and more lateral to improve the view of the omentum and right upper quadrant. The epigastric working port would be placed just to the right of midline to allow a safe, cephalad vector for omental adhesiolysis. I'd place the right subcostal ports slightly more lateral than usual to optimize traction vectors on the gallbladder and liver. Before any dissection begins, I'd clear omental adhesions first with careful blunt and low-energy dissection to establish a safe plane and improve visualization of the gallbladder. Because the hepatic flexure is not involved, I'd avoid unnecessary colonic mobilization; instead, I'd use gentle fundal retraction and lateral-inferior traction on the infundibulum to open up the triangle. With the adhesion load limited to the body, I'd proceed with standard dissection of the peritoneum and areolar tissue, reserving energy only for precise, short bursts to avoid thermal spread near the duodenum. Throughout, I'd maintain a low threshold for intraoperative cholangiography if the pedicle remains obscured or if there's any doubt about the anatomy. Bailout strategies—such as subtotal cholecystomy or conversion—are unlikely to be needed here because exposure can be achieved with standard techniques and the risk profile is favorable.

{'Correctness': 97, 'Relevance': 94, 'Linguistic': 96}

Fig. 12: Qualitative comparison of model responses on reasoning-level tasks. The figure illustrates how our SurgTEMP generates comprehensive detailed descriptions and performs complex hypothetical reasoning about surgical scenarios, demonstrating superior temporal understanding and clinical reasoning capabilities compared to baseline models.

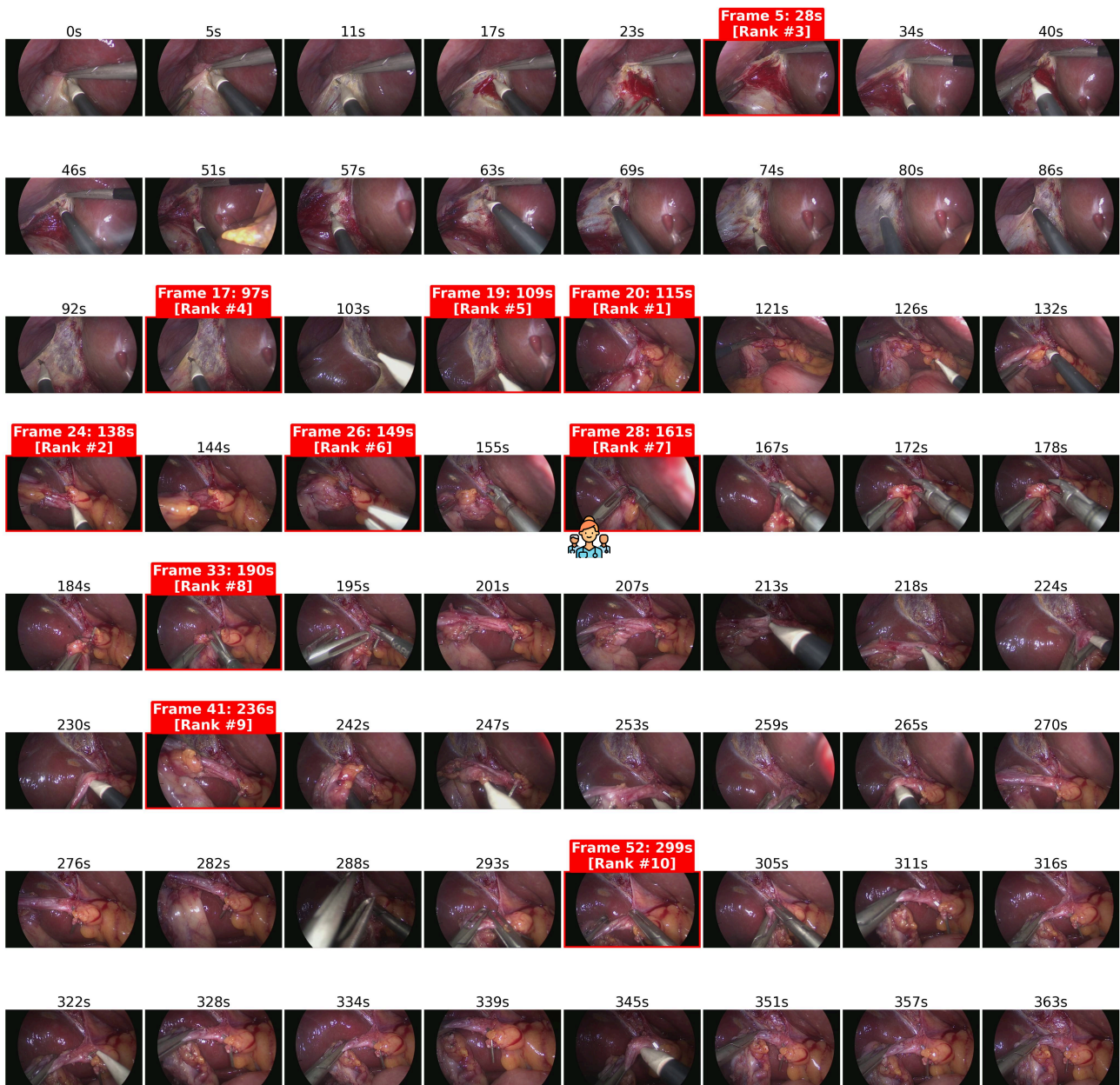


Question: Is the falciform ligament noticeably fat-laden here, and how does that influence port planning?

Ground Truth Answer: It appears prominent and may restrict direct subxiphoid port placement; adjusting placement can mitigate this.

Our Model Generated Answer: Yes. The falciform is bulky and fatty, which can obscure the epigastric view and interfere with subxiphoid port placement. I'd plan for a slight adjustment of the epigastric port or consider a suspension suture to keep it out of the way.

Fig. 13: Visualization of the frame selection process in the TEMP module. Sixty-four frames are displayed in an 8x8 grid with timestamps shown above each frame. Ten selected frames are highlighted with red bounding boxes showing their rank during top-k selection. The most informative frame selected by a clinical expert is indicated with an icon in the bottom-left corner. Question, ground truth answer, and generated answer are shown below the frame grid.



Question: Do you see evidence of thermal injury during the bed dissection, and if so, how would you characterize it?

Ground Truth Answer: Yes. There's a minor, superficial thermal contact on less vital tissue, suggested by a faint blanching/singe without structural damage. It's an isolated event without impact on critical structures.

Our Model Generated Answer: Yes. There is minimal, superficial thermal effect limited to non-critical tissue, with slight discoloration and no structural or functional impact.

Fig. 14: Visualization of the frame selection process in the TEMP module. Sixty-four frames are displayed in an 8x8 grid with timestamps shown above each frame. Ten selected frames are highlighted with red bounding boxes showing their rank during top-k selection. The most informative frame selected by a clinical expert is indicated with an icon in the bottom-left corner. Question, ground truth answer, and generated answer are shown below the frame grid.